HELSINKI UNIVERSITY OF TECHNOLOGY
Faculty of Electrical Engineering

Mikko Syrjäsuo

All-sky camera

1.4.1996

Master's Thesis which has been submitted for revising for the degree of Master of Science in engineering.

Supervisor: Ass. prof. Olli Simula

Instructor: Doc. Tuija I. Pulkkinen

Please note FMI/GEO all-sky camera WWW-pages at
http://www.geo.fmi.fi/∼syrjasuo/asc_index.shtml

HELSINKI UNIVERSITY OF TECHNOLOGY

ABSTRACT OF THE MASTER'S THESIS

Author: Mikko Syrjäsuo

Title of the thesis: All-sky camera

Title in Finnish: Revontulikamera

Date: 1st April 1996 **Number of pages:** 67

Department: Faculty of Electrical Engineering

Professorship: Tik-61 Information Science

Supervisor: Ass.Prof. Olli Simula

Instructor: Dr. Tuija I. Pulkkinen

Aurora borealis is caused by charged particles that originate from the Sun and interact with the air molecules in the upper atmosphere. The excited molecules emit radiation at wavelengths in the visible spectrum. The various colours of aurorae emerge from different excitation states.

So far no-one has succeeded in simulating the environment of the upper atmosphere in laboratory conditions. Thus the only way to study the phenomena which occur at an altitude of approximately 100km is to perform observations either with ground-based or satellite-borne instruments.

Finnish Meteorological Institute (FMI) has traditions in aurora borealis research: earliest observation summaries were written in the 18th and 19th centuries. FMI's all-sky camera network was started in the 1970's, and today there is a collection of approximately two millions images of aurorae. An all-sky camera uses a special lens configuration in order to image the whole visible sky at once.

The old cameras need to be replaced with new ones within the next few years. In this work the requirements for these modernised all-sky camera stations were first created –special care was taken to fulfill the needs of the scientists. A prototype station was built which consisted of a computer controlled imaging instrument. The somewhat lower requirements for the prototype as well as design and operation of the prototype itself are presented.

The prototype was tested by imaging aurorae, and preliminary test results are shown. Most of the previously set requirements were met; suggestions to improve weaker performance in some details are presented.

Keywords: Aurora borealis, space plasma physics, image acquisition

TEKNILLINEN KORKEAKOULU **DIPLOMITYÖN TIIVISTELMÄ**

Tekijä: Mikko Syrjäsuo

Työn nimi: Revontulikamera

Title in English: All-sky camera

Päivämäärä: 1.4.1996 **Sivumäärä:** 67

Osasto:
Sähkötekniikan osasto

Professuuri:
Tik-61 Informaatiotieteet

Työn valvoja: Apul. prof. Olli Simula

Työn ohjaaja: Dos. Tuija I. Pulkkinen

Revontulet syntyvät ilmakehän yläosissa, kun auringosta peräisin olevat varatut hiukkaset törmäävät ilmamolekyyleihin. Molekyylit luovuttavat osan viritysenergiastaan säteilemällä näkyvän valon alueella. Revontulten eri värit johtuvat juuri erilaisista viritystiloista.

Ilmakehän yläosien olosuhteita ei toistaiseksi pystytä luomaan laboratorio-olosuhteissa, joten ainoa keino tutkia noin 100 kilometrin korkeudella tapahtuvia avaruusplasmafysiikan ilmiöitä on tehdä joko maanpäällisiä tai satelliittimittauksia.

Ilmatieteen laitoksella on perinteitä revontulitutkimuksen alueella: havaintojen yhteenvetoja on 1700- ja 1800-luvuilta alkaen. Laitoksen revontulikameraverkko aloitti toimintansa 1970-luvulla, ja tällä verkolla on kerätty tähän mennessä noin kaksi miljoonaa revontulikuvaa. Kuvat ot etaan linssijärjestelmällä, joka mahdollistaa koko näkyvän taivaankannen kuvaami sen kerralla.

Tässä työssä luotiin aluksi vaatimukset modernisoiduille revontulikamera-asemille, joilla vielä toiminnassa olevat vanhat kamerat on tarkoitus korvata. Vaatimuksissa pyrittiin huomioimaan tutkijoiden tarpeet mahdollisimman hyvin. Työtä jatkettiin rakentamalla aseman prototyyppi, joka koostuu tietokoneen ohjaamasta kuvausinstrumentista. Prototyypin vaatimukset, tehdyt ratkaisut sekä prototyyppi esitellään.

Prototyyppiä koekäytettiin todellisissa toimintaolosuhteissa, ja testien tuloksia esitellään. Prototyyppi täytti pääosin esitetyt vaatimukset, ja testeissä ilmenneisiin puutteisiin esitetään parannusehdotuksia.

Avainsanat: Revontulet, avaruusplasmafysiikka, kuvankäsittely

Preface

This work has been done at Geophysical Research of Finnish Meteorological Institute. I would like to thank all my colleagues for creating such a joyful and encouraging working atmosphere, and I would like to thank the head of the department Prof. Risto Pellinen for the most interesting work that was offered to me.

My special thanks go to my instructor Dr. Tuija Pulkkinen who patiently introduced the world of auroral physics to me. Numerous problems that seemed mysterious to me were actually quite logical, after all.

I would also like to thank the rest of the all-sky camera team: Dr. Asko Huuskonen, Dr. Arja Pajunpää, and Dr. Kirsti Kauristie who were always ready to answer even to the most strangest questions. In addition to the camera team, I would like to thank the head of the space physics group Dr. Hannu Koskinen who had time and interest to discuss the development of the prototype.

I spent two most interesting weeks as a guest of Swedish Space Physics Institute in Kiruna. Their auroral imaging team kindly provided one of their domes for testing the all-sky camera prototype; I had many fruitful discussions with ke Steen, Björn Gustavsson and especially with Urban Brändström.

Last but not least, I would like to thank Prof. Gilbert Leppelmeier who kindly corrected not only punctuation marks in English but also made very useful comments.

Helsinki, 1.4.1996

Mikko Syrjäsuo

Contents

Preface **4**

Notations and symbols **8**

1. Introduction **11**
1.1 Background 11
1.2 Introduction to this work 11

2. Aurora Borealis **13**
2.1 Historical review 13
2.2 Scientific explanation 13
2.2.1 Geomagnetism and solar wind 13
2.2.2 Auroral oval 14
2.2.3 Substorms 15
2.3 Auroral observations 16
2.3.1 The unit Rayleigh 16
2.3.2 Ground-based observations 16
2.3.3 Satellite observations 17
2.3.4 Observation programmes at Finnish Meteorological Institute 17

3. Requirements for the new all-sky camera **21**
3.1 Station network 21
3.2 All-sky camera station 21
3.2.1 Introduction 21
3.2.2 Local environment 23
3.2.3 Optics and the camera element 23
3.2.4 Camera housing and housekeeping electronics 23
3.2.5 Computers 24
3.2.6 Software 24
3.3 Network operation 24
3.4 Requirements for the prototype 25
3.4.1 Environment 25
3.4.2 Hardware 25
3.4.3 Software 25

4. The station prototype **27**
4.1 Overview . . . 27
4.2 Optics . . . 27
4.3 Prototype Housing . . . 29
4.4 Computer . . . 29
4.4.1 Operating system . . . 29
4.4.2 Computer hardware . . . 30

5. The station software **29**
5.1 Image acquisition . . . 29
5.2 Image data processing . . . 29
5.3 Housekeeping routines . . . 31
5.4 Control Centre Software . . . 33
5.4.1 Imaging control . . . 33
5.4.2 Image data handling . . . 34

6. The imager **36**
6.1 Overview . . . 36
6.2 Optics . . . 36
6.2.1 Fish-eye lens . . . 36
6.2.2 Shutter and filter wheel . . . 37
6.2.3 Image intensifier . . . 37
6.2.4 CCD camera . . . 38
6.3 Controlling the all-sky camera . . . 38
6.4 Corrections and calibration . . . 38
6.4.1 Dark current and read-out noise . . . 38
6.4.2 Flat-field correction . . . 39
6.4.3 Geometrical alignment and calibration . . . 40
6.4.4 Brightness calibration . . . 40

7. Test results **41**
7.1 Laboratory tests at FMI/GEO . . . 41
7.2 Hankasalmi 14.–18.2.1996 . . . 41
7.3 Tests in Kiruna 3.–14.3.1996 . . . 43
7.3.1 Test set-up . . . 43
7.3.2 Operating the prototype . . . 43
7.3.3 Performance measurements . . . 43
7.4 Image compression . . . 47
7.5 Auroral observations . . . 47

8. Summary and conclusions **50**
8.1 Prototyping results . . . 50
8.2 Further development . . . 50
8.3 Decisions . . . 51

References **51**

A Projecting an image onto a map **54**
A.1 Map projection 54
A.2 Finding corresponding points in the image and on the map 56

B Measuring optical radiation **59**
B.1 Irradiance, radiant intensity and radiance 59
B.2 Optical terminology 62
B.3 Sensor readings 63

C Station software details **66**
C.1 Dayschedule file 66
C.2 User interface 67
C.3 Frame grabber routine front-end 68

Notation and symbols

The notations and symbols used in this work are listed here.

AE	Auroral Electrojet.
ALIS	Auroral Large Imaging System.
ASC	All-sky camera.
CCD	Charge coupled device.
DAT	Digital audio tape.
DDS2	Digital data storage standard for DAT.
EISCAT	European Incoherent Scatter Radar.
ESA	European Space Agency.
FMI	Finnish Meteorological Institute.
FMI/GEO	Finnish Meteorological Institute, Geophysical research.
FOV	Field of view. In general this indicates the solid angle that can be seen. The *angular* FOV is the top angle of the cone formed by the solid angle.
GG	Geographical (e.g. coordinates)
IGY	International Geophysical Year.
IMAGE	International Monitor for Auroral Geomagnetic Effects.
ISDN	Integrated service digital network.
Keoitt	An old Eskimoan word for aurora borealis.
MLT	Magnetic local time.
PC/AT compatible	A computer model that is compatible to IBM PC/AT computer.
PC/104	A standard for industrial PC/AT compatible computer espesially suited for embedded applications.
R	Rayleigh, $1\mathrm{R} = 10^6 \mathrm{photons/cm^2/s}$.

STARE	Scandinavian Twin Auroral Radar.
TCL/TK	Tool command language/toolkit.
UPS	Uninterruptible power supply.
UT	Universal time.
UTC	Coordinated Universal Time.
WTS	Westward travelling surge.
a	x coordinate of an image point in the image matrix.
$\mathbf{B}$	Magnetic field.
B	Brightness.
b	y coordinate of an image point in the image matrix.
C	Image matrix.
C_{exp}	Expected count per pixel per second.
C_S	Measured count (including the signal count).
C_T	Background count.
ΔC	The number of rayleighs described by one count.
$\Delta\widehat{C}$	The estimated number of rayleighs described by one count.
d	Radius in the polar coordinates of a point in the image matrix.
$\mathbf{E}$	Electric field.
$\mathbf{F}$	Force.
f	Focal length.
$\mathbf{j}$	Current density.
L_s	Source radiance.
M	Map matrix.
q	Charge of a particle.
$\mathbf{r}(\theta, \varphi)$	A vector pointing from the centre of the Earth to the point where the latitude is θ and the longitude is φ.
R_E	The radius of the Earth, approximately 6370km.
$\mathbf{v}$	Velocity.
W	The width of the filter.

X	x coordinate of a point projected onto the map plane.
Y	y coordinate of a point projected onto the map plane.
θ	Latitude.
σ	Conductivity.
ϕ	Angle in the polar coordinates of a point in the image matrix.
φ	Longitude.
Ψ	The angle between the incoming ray and the optical axis in an optical system.

1. Introduction

1.1 Background

In the space around the Earth numerous complicated electrodynamic processes take place. In these processes charged particles interact with each other and move under the influence of electromagnetic forces. The physics of gas consisting of neutral and charged particles is generally called *plasma physics*; it has been estimated that approximately 99.9% of the matter in the Universe is in a plasma state.

The most energetic particles originate from the Sun, and the increasing activity of the Sun can be observed as subsequent changes in the Earth's magnetic field. Aurora borealis —the northern lights— are caused by charged particles that flow along Earth's magnetic field lines to high northern and southern latitudes. The particles interact with the ions in the upper atmosphere at an altitude of approximately 110km, and when the excited particles transit back to the ground-state aurorae are generated.

Unfortunately, no-one has so far succeeded in simulating the tenuous plasma environment of the upper atmosphere in laboratory conditions, and the only way to study the plasma around the Earth is to perform observations by ground-based or satellite instruments. Examples of these instruments are photometers, all-sky cameras, auroral radars, and magnetometers. Current trend is that special campaigns are arranged where different instruments measure simultaneously —for example, in-situ satellite observations are complemented by remote ground-based observations— and the various measurements are combined to create a more accurate picture.

1.2 Introduction to this work

This work has been carried out in the space physics group in the Geophysical Research of Finnish Meteorological Institute (FMI). The work concerns a new all-sky camera design which will later replace the current all-sky cameras manufactured in 1970's. An all-sky camera (ASC) can image the whole visible sky by using special lens configurations; the majority of today's all-sky cameras exploit fish-eye lenses. By using several ASCs global cover over Finnish Lapland can be achieved.

In this work a prototype all-sky camera station was designed and operated in real situations. Much of the time was spent in formulating the requirements for the new stations; the solution had to be a compromise between image quality and expenses while guaranteeing scientifically useful measurements. Reliable automated operations is required as well. At this stage of development the emphasis was on

individual station details, but a few global requirements were also formulated.

In Chapter 2 an introduction to the physics of aurorae is given. Furthermore, the fundamental auroral instruments are also described. Chapter 3 discusses the requirements set to the new all-sky camera station, and the station hardware is presented in Chapter 4. Description of the current preliminary station software is given in Chapter 5. The camera optics, necessary electronics, and image processing guidelines are discussed in Chapter 6. Chapter 7 describes the results of laboratory and field-tests performed during the spring of 1996. Summary and discussion of further work are presented in Chapter 8.

2. Aurora Borealis

2.1 Historical review

Perhaps the first description of *aurora borealis* in literature was written by Aristoteles: in his book *Meteorologica* he described phenomena he had seen in 349 and 344 Bc. According to Aristoteles the world consisted of four elements: fire, air, water and land. The aurora borealis could be explained by the heat of the Sun, which extracted steams out of land, and these steams then collided with fire and caused flames. When these flames penetrated air, colours were emitted.

The name aurora borealis, "the red northern sky at dawn", was invented by a French mathematician and astronomer Pierre Gassendi when he was observing the Northern sky above Paris in September 1621. Correspondingly there are *aurora australis* in the southern hemisphere, and captain James Cook was among the first who wrote notes about them in 1770.

In the 19th century people started to understand that the aurora borealis evolve from processes in the Earth's atmosphere. Scientists began to make colour drawings and illustrations that were published in scientific journals and books. This effort culminated during the first large international observation period called The First Polar Year (1882–1883), but inspite of numerous efforts no photographs were available at that time. Only in 1892 a German photographer M.Brendel made the first photograph of aurora borealis; the first colour photographs were made public in a scientific meeting 60 years later in 1951.

Before the International Geophysical Year (IGY) in 1957–58 many of the unresolved problems were explained: the main light source was the emission radiation from oxygen atoms excited by the particles originating from the Sun, and the concept of *auroral ovals*, to where the particles from the Sun arrive from the Earth's magnetosphere, was introduced. During IGY a network of 144 all-sky cameras was operated, which allowed the characterisation of the spatial and temporal evolution of the auroral activity. The understanding of auroral phenomena has increased with satellite based instruments both in the upper atmosphere and in the magnetosphere.

2.2 Scientific explanation

2.2.1 Geomagnetism and solar wind

The Earth's magnetic field is produced by a self-exciting dynamo in its liquid core. The generated field can be approximated by a magnetic dipole, but at high altitudes the solar wind and its embedded magnetic field distort the dipolar shape. The

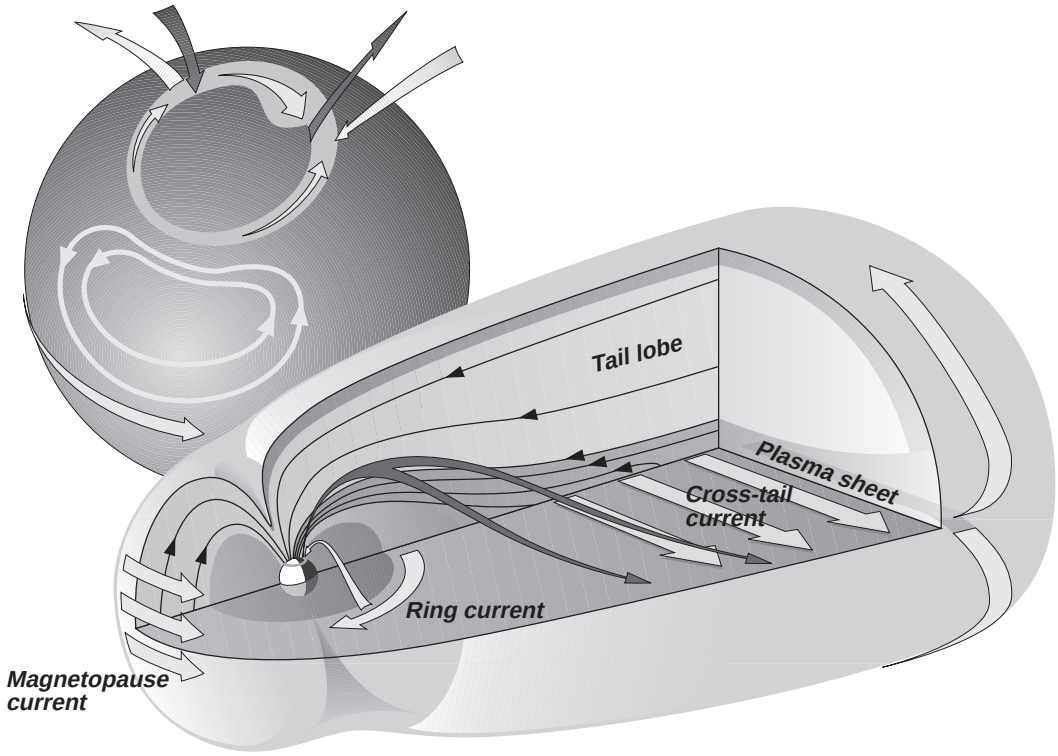

Figure 2.1: The Earth's magnetosphere.

magnetosphere is the region of space around the Earth within which the magnetic field of the Earth is confined by the solar wind. Ionised particles originating from the Sun interact with the Earth's magnetosphere under the Lorentz-force[1] and due to the configuration of the velocity of the particles and the direction of the magnetic field, various current systems within the magnetosphere are formed.

Figure 2.1 illustrates the Earth's magnetosphere. The Sun is to the left and the solar wind affects the shape of the magnetosphere. The length of the *magnetotail* varies —according to some observations it can extend beyond $200R_E$, where R_E is the radius of the Earth (6370km). A *ring current* is created by electrons and ions drifting in opposite directions in the quasi-dipolar region near the Earth.

Affected by variation in the solar wind and its embedded magnetic field, the magnetospheric magnetic field changes in time. This is called *magnetic activity*.

2.2.2 Auroral oval

The auroral oval is defined at any time instant as the roughly circular region around the magnetic poles within which aurorae are observed. The auroral ovals are magnetically connected to a region in the magnetotail called the *plasma sheet* where plasma density is higher than in the enveloping tail lobe . From the plasma sheet particles continuously flow along the magnetic field lines to high northern and southern latitudes, where they interact with the ionosphere and generate aurorae.

[1] $\mathbf{F} = q(\mathbf{E} + \mathbf{v} \times \mathbf{B})$, where q is the charge of the particle, $\mathbf{E}$ the electric field, $\mathbf{v}$ the velocity($\ll c$), and $\mathbf{B}$ the magnetic field.

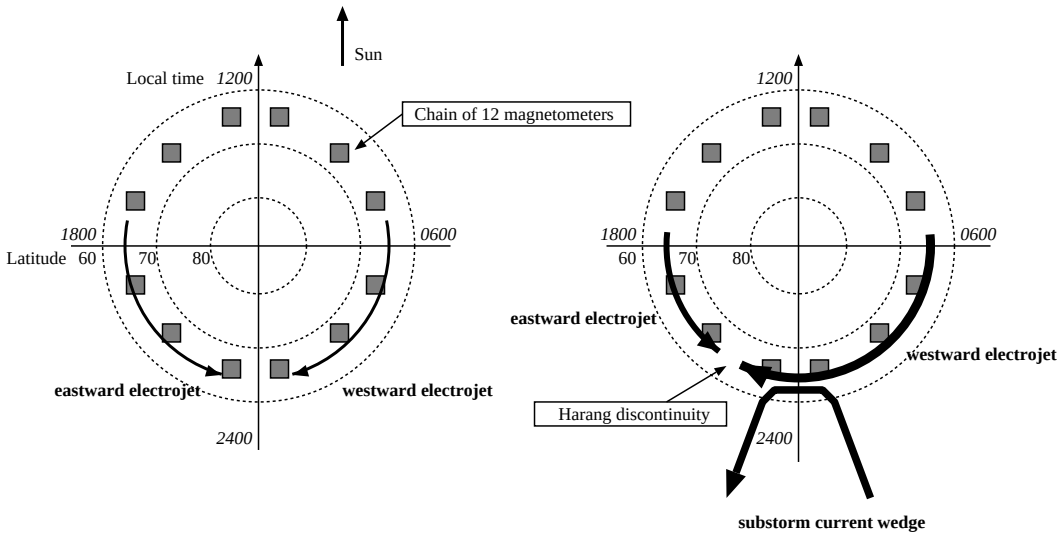

Figure 2.2: The electrojets.

The size and shape of the auroral oval is not constant. Two different types of aurorae can be distinguished: *discrete aurora* and *diffuse aurora*. The discrete aurorae appear as single bright arcs that are separated from others by dark spaces. The diffuse aurorae form a broad band of auroral luminosity whose width is at least several tens of kilometers. Typically the discrete aurorae appear in the poleward part of the oval, whereas the diffuse aurorae are observed in the more equatorward part of the oval.

Figure 2.2 illustrates the auroral oval region seen above the north pole. In the auroral oval there are two major current systems, the *eastward* and *westward electrojets*. These electrojets affect the Earth's magnetic field, and an international magnetometer chain consisting of 12 station is used in generating the AE-indices (Auroral Electrojet). Each station measures the strength of the Earth's magnetic field —which is disturbed by the time-varying electrojets— and the AE-index is calculated by taking the difference of the minimum and the maximum value among the stations. "Zero condition" is the average of five quietest days of the month, and the time step in the AE-index is one minute.

The substorm current wedge connects the ionospheric and magnetospheric current systems near local midnight during periods when both auroral and magnetic activity are observed.

2.2.3 Substorms

A magnetospheric substorm is a process during which energy extracted from the the solar wind is first stored in the magnetotail and later released through an explosive instability growth. At the auroral latitudes, bright auroral displays are accompanied with several 100nT disturbances in the surface magnetic field.

A substorm is usually divided into three distinct phases:

- the growth phase,

- the expansion phase,
- the recovery phase.

A typical substorm lasts 1–3 hours, although in many cases it is very difficult to distinguish subsequent substorms from each other.

During the *growth phase* solar wind energy is loaded into the magnetotail. In the auroral regions, discrete arcs appear and begin to drift equatorward. *Pseudo-breakups* are frequently observed. Pseudobreakups are localised auroral activations that usually last only $\sim$ 5min.

At the *expansion onset* the most equatorward auroral arc suddenly brightens. This brightening expands poleward and fills the region behind it with rapidly moving turbulent aurorae. The duskward edge of this bulge forms a wave-like disturbance called the *westward-travelling surge* (WTS) that appears to propagate along the previously brightened arc. The poleward, westward and eastward propagation typically lasts for 30–60min.

Eventually these expansions stop and quiet auroral arcs begin to reform in the *recovery phase*. At the equatorward edge of the morningside auroral oval, arcs break into eastward-drifting pulsating patches or omega-shaped structures. The duration of the recovery phase is typically 60–120min.

2.3 Auroral observations

2.3.1 The unit Rayleigh

A photometric unit for (apparent) radiance used in airglow and auroral measurements is one *rayleigh* [R]. The unit was first introduced by *Hunten et al.* [*1956*]. They proposed that the measurement results should be reported in terms of $4\pi B$, rather than the measured surface brightness B itself. This multiple of $4\pi B$ should then be called rayleigh when B is in units of 10^6 quanta /cm^2 s sr. Nowadays, the definition is usually given for its use as a generalised unit of apparent radiance [*Huffman, 1992*]

$$1\,R = \frac{10^6 \text{ photons}}{s\ \text{cm}^2(4\pi\ \text{sr})(\Delta\lambda)}, \tag{2.1}$$

where $(4\pi\, sr)$ and $(\Delta\lambda)$ emphasise the omnidirectional emission and the dependence on the wavelength.

2.3.2 Ground-based observations

The most important ground-based optical instruments are all-sky cameras, special TV cameras and auroral photometers. The sensitivities and purposes of various optical instruments are given in Table 2.1.

All-sky cameras typically cover an area of about 600km in diameter, and the imaging frequency is few images per minute. TV cameras have faster time resolution but a more limited field of view. Photometers provide also spectral information from either a single point or a single meridian.

2.3.3 Satellite observations

Several satellites in the past have been used in auroral observations. One advantage of satellites is that one image can cover the whole auroral oval, which is not possible with ground-based instruments.

Satellites in an 800km (or 100 min) orbit can produce one image per orbit, and one example of them is the *DMSP*-programme (USA), which is currently active. The apogee of *Dynamics Explorer-1* (launched 1981) is at $4R_E$, and it produced oval images at 12-min intervals. A Swedish *Viking* (1985–86) produced oval images at 20-s interval, whereas *Freja* (1992) imaged parts of the oval at 6-s interval.

2.3.4 Observation programmes at Finnish Meteorological Institute

The ionospheric electrodynamics is largely governed by Ohm's law

$$\mathbf{j} = \sigma \mathbf{E}, \tag{2.2}$$

where $\mathbf{j}$ is the current density, σ the conductivity and $\mathbf{E}$ the electric field. By using different instruments each of the factors in (2.2) can be observed independently. By using magnetometer measurements the value of $\mathbf{j}$ can be deduced, $\mathbf{E}$ can be obtained from radar observations, and σ can be indirectly estimated from auroral all-sky images.

The all-sky camera (ASC) chain operated by Finnish Meteorological Institute (FMI) was started in the 1970's. A time serie of images produced by one ASC is shown in Fig. 2.3. These cameras have now been operational for more than twenty years; currently there are three cameras in Finnish Lapland and one in Svalbard. The locations of the ASCs are shown in Table 2.2.

A common analysis tool for auroral research is a keogram. A keogram is a time versus latitude plot composed of (magnetic) north-south aligned lines of all-sky images. Showing the latitudinal evolution of auroral motions, the keogram provides a quick way to find interesting time periods for more detailed studies. An example of a keogram is shown in Fig. 2.4.

Table 2.1: Instruments for ground-based auroral observations.

Instrument	Sensitivity	Exposure	Use
Human eye	1 kR		
All-sky film camera	0.5–1.0 kR	1-30 s	continuous monitoring
All-sky CCD camera	<100 R	1-10 s	continuous monitoring
Keogram camera	50 R	continuous, moving film	meridional auroral motions especially dayside aurora
TV-camera	50 R	1-50 frames/s	rapid variations
Auroral photometer	few R		quantitative measurements of individual auroral structures

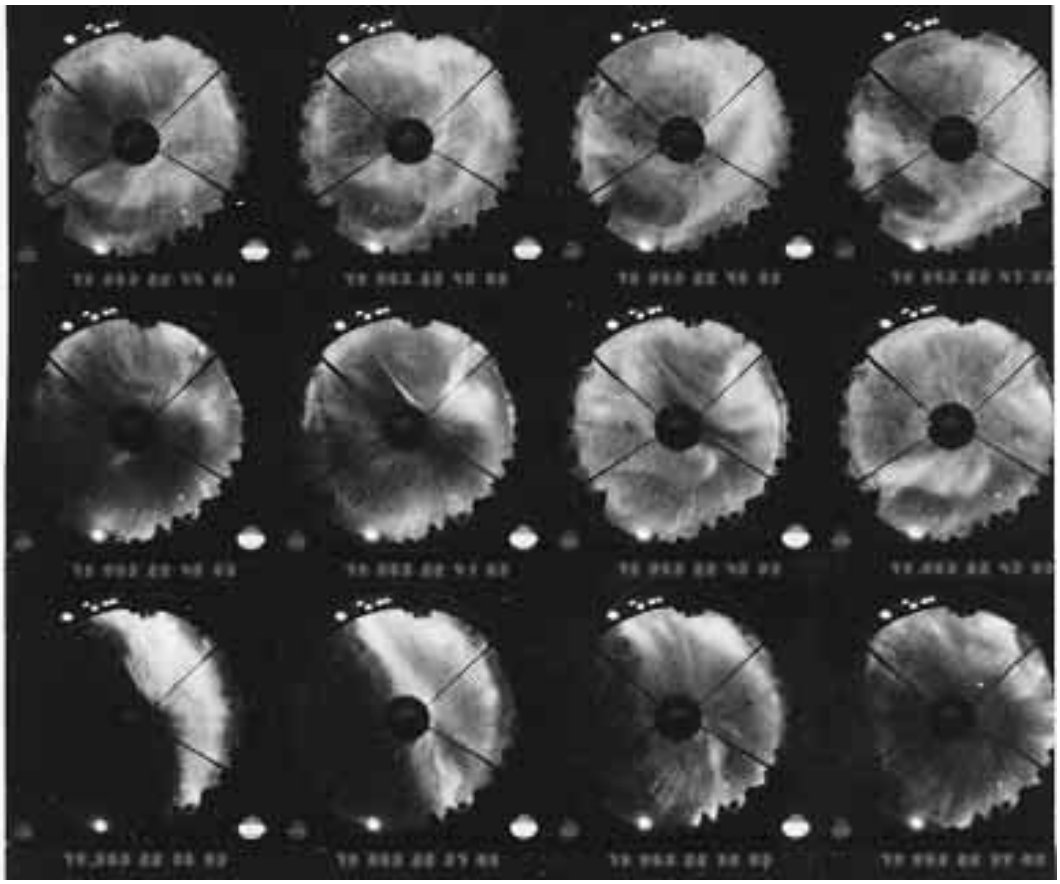

Figure 2.3: A serie of all-sky images.

Table 2.2: Finnish ASC network. Station locations are given in geographic coordinates.

Station	GG Lat	GG Lon
Muonio	68.028N	23.563E
Kevo	69.749N	27.021E
Kilpisjarvi	69.020N	20.864E
Hornsund	77.000N	15.600E

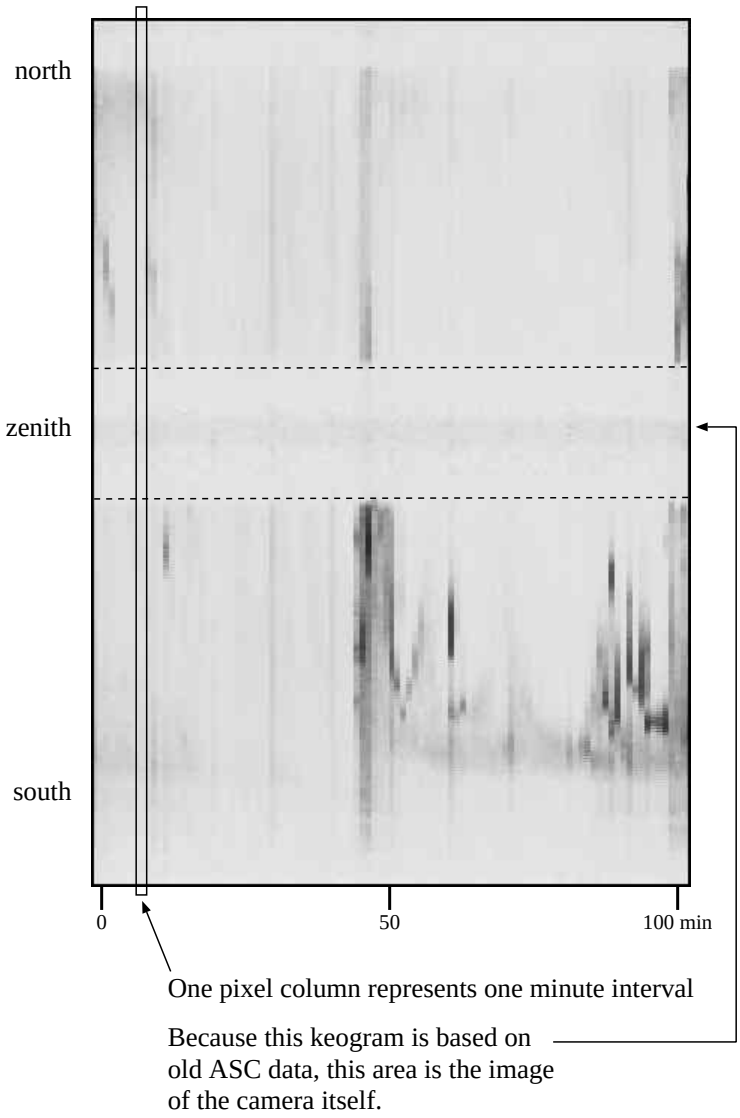

Figure 2.4: A keogram (negative greyscale).

In addition to the all-sky camera network, FMI operates a magnetometer chain called IMAGE (International Monitor for Auroral Geomagnetic Effects). The latitudinal chain records the variations in the surface magnetic field, which can be used to infer the ionospheric current intensities and locations.

In co-operation with other European countries Finland has contributed to the EISCAT-radar for more than ten years. EISCAT (European Incoherent Scatter) radar monitors the ionospheric particle densities and flows in the auroral oval region.

STARE (Scandinavian Twin Auroral Radar) consists of two radar stations, one in Malvik in Norway and the other in Hankasalmi, Finland. By combining the line of sight measurements from the two radars it is possible to map the electric field pattern over a large area over the auroral region.

In future the emphasis will be on large international co-operative observation programmes. The ground observations complement satellite measurements such as those made by ESA's (European Space Agency) CLUSTER programme to be launched during 1996. This combination of instruments facilitates the study of the boundaries of the magnetosphere and the development of substorms in the magnetotail.

3. Requirements for the new all-sky camera

3.1 Station network

The all-sky camera network built by Finnish Meteorological Institute in the early 1970's consists of several all-sky camera stations in Northern Finland. At this moment there are three operational stations, located in Kilpisjärvi, Kevo and Muonio. In addition to these there is one station in Hornsund (Svalbard).

Figure 3.1 shows the area observed by the current stations in Finland. One station covers a circular area whose diameter[2] is approximately 600km. The new station network should cover at least the same area, and in order to utilise the already existent station buildings, the new cameras should be placed to the same locations as the old cameras.

3.2 All-sky camera station

3.2.1 Introduction

The all-sky camera described in this work is a prototype. Some of the components used are less expensive than those that will be used in the operational model, and parts of the software is still preliminary. The exact models and component types will be chosen after the prototype has been thoroughly tested.

The general performance is evaluated by using the prototype in real situations, and by measuring the sensitivity in laboratory conditions with light standards. A comparison test against old all-sky cameras will be performed; image quality is subjectively rated.

The prototype software consists of image handling and storing software, timekeeping processes, and housekeeping routines. The image handling and storing routines control the camera electronics and store the image data. Timekeeping processes take care of daily activities (such as imaging schedule), while housekeeping routines monitor the status of the all-sky camera station. Additionally, there is some network software that is used in evaluating the network operation, such as automatic transmission of housekeeping data and image data transfer from the station to a remote computer.

[2] Calculated by using a field of view of 160°.

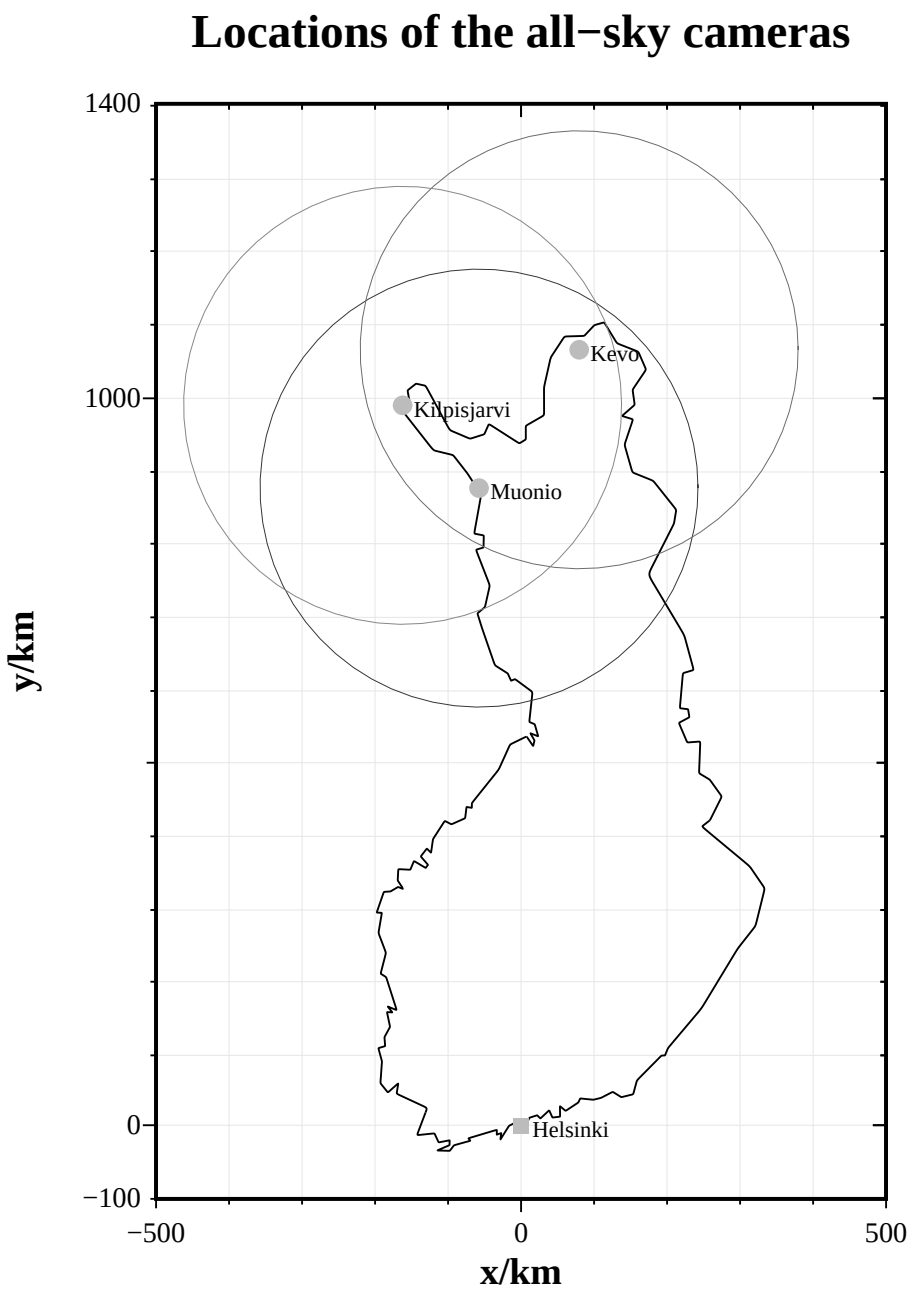

Figure 3.1: Old all-sky camera stations.

3.2.2 Local environment

Because the old stations have been operational for several years, placing a new camera requires basically only changing camera hardware. Even though the actual camera and optics are placed outside, the controlling computer is held in room temperature in a nearby station building. The distance between the camera and the computer can be up to 30 meters.

All the current ASC stations are part of a bigger, local scientific measurement station, and service personnel can perform routine operational checks.

3.2.3 Optics and the camera element

The old all-sky cameras use ordinary film cameras for imaging and the sensitivity is $\sim 600 - 700$R, somewhat better than the human eye. In order to observe faint auroral phenomena the new camera should be able to detect much smaller radiances in the range of $100 - 200$R. Naturally, a more sensitive equipment is also more expensive and a price-performance compromise is required.

There are two commonly used methods for all-sky imaging: the one uses a fish-eye lens and the other has a spherical mirror that the camera images. In both cases an all-sky image is obtained with an angular field of view (FOV) of approximately 180° (ie. the solid angle is 2π), but in the latter configuration the centre of the image is blocked by the camera. Usually the losses in the mirror configuration are smaller than in the fish-eye lens, and a less sensitive imaging camera is needed.

Modern optical instruments frequently use charge coupled devices (CCD) as sensors, thus using a CCD camera is a natural choice. Because colour cameras are considerably more expensive and also less sensitive, the baseline was to select a monochrome integrating camera. Integrating in this case means that the exposure time can be longer than the usual video rate (1/25 s); the camera can thus collect photons for several seconds if needed. By using monochrome imaging one cannot separate different emission wavelengths, and thus a controllable filter wheel accommodating several filters should be included in the design.

The spatial resolution requirement was set to 512 times 512 pixels digitised to 8 bits. This resolution was considered to be sufficiently accurate for global auroral movement and auroral arc form studies. The resolution is for the most part set by the capacity of data storage. Estimated data rates are shown in Table 3.1.

3.2.4 Camera housing and housekeeping electronics

Although the controlling computer is at room temperature, the actual camera has to survive local weather conditions which can be very rough at the latitudes of the stations. An insulated housing will be manufactured with a transparent dome at the top through which the camera can see the sky. The housing requires temperature control and the dome is kept clear by letting heated air circulate inside.

Some of the electronics will be mounted inside the camera housing. For example, most of the CCD camera controllers need to be placed next to the camera. In addition to the necessary control electronics a small set of housekeeping sensors is needed. The purpose of the housekeeping electronics is to be able to detect possible

Table 3.1: Estimated image data amounts

Amount of images	**Uncompressed data**	**Size of three images taken through filters**
One $512 \times 512 \times 8$ image	256kB	768kB
One complete imaging cycle (duration 14 hours, interval between images is 20 seconds ($\Rightarrow$ 2520 images)	630MB	1.9GB
One imaging week	4.3GB	13.2GB

hardware problems arriving from, for example,sudden temperature drops due to too thin insulation.

All electrical lines coming from the camera housing should be protected. The required power supplies should have current limiters, and the power should come through an uninterruptible power supply (UPS). All connection cable connectors should be targeted for outdoors use.

Service operations in field should be made easier by arranging the components inside the camera housing in a modular fashion. If major operations are required, the whole housing will be carried inside.

3.2.5 Computers

At least one computer at each camera station is needed for controlling the operation and storing the image data. This computer should autonomously start and stop imaging, check housekeeping measurements, store data and notify errors to service personnel. In order to control all all-sky camera stations centrally this camera computer should be connected to a network. For easy replacement, the chosen computer should be commonly available and use as many standard components as possible.

3.2.6 Software

The software can be divided into two sections: local software that runs at the stations and remote control software that is operated from elsewhere. In the case of the prototype the emphasis is on the local software.

The camera computer should take care of the actual imaging, ie. the image acquisition, data compression and storing. The operations should be based on pre-programmed timetables or remote commands. Automatical health-check messages to service personnel should be sent at fixed time intervals or when necessary.

3.3 Network operation

The operation of every all-sky camera station is controlled by FMI, accomplished by forming a computer network. Generally the network operator will be in Helsinki;

through accessing a selected all-sky camera station remotely the operator should be able to fully control the station. Some important possibilities are uploading new station software and new operation timetables. Although it is possible to transfer image data via networks, it is not practical due to the vast amount of data —at least not by using modems. Downloading test images should be possible for operational tests.

Every individual camera station should be able to send messages through the network automatically. Examples of these automatically generated messages are malfunction reports and statistical data such as images composed of excerpts of all images.

Possible choices for the network hardware are modems, direct *Ethernet* connections or *ISDN* modules.

3.4 Requirements for the prototype

3.4.1 Environment

Testing of the prototype all-sky camera can be done in a thermally controlled environment which means that no insulated housing is required. A suitable testing location is in Hankasalmi, where a building with a transparent dome at the roof is at FMI's disposal. Similar conditions are provided at Nurmijärvi Geophysical Observatory.

The exact requirement for the insulated housing and the size of the dome (see chapter 3.2.4) will be determined after the specific hardware decisions are made. For example, some new components may be required due the electrical interferences.

3.4.2 Hardware

The prototype hardware consists of the camera with suitable optics and the station computer. Because the prototype camera and computer can be kept close to each other, no signal line amplifiers are required. However, the effect of an amplifier on the signal quality should be studied.

The computer should have a frame grabber card or other additional hardware to digitise the captured images. Also, a suitable mass storage and communication hardware are needed.

3.4.3 Software

The prototype software will mostly consist of routines dedicated for station operation. The most important routines are the imaging routines, which control the frame grabber and store the image data. Each image should be labelled with a timestamp consisting of the time of day and date. The time interval between consequent images and the exposure time are given in a timetable.

In addition to the imaging, some daytime operations are needed. The image data has to be transferred into a mass media, and daily statistics should be generated, some of which should be send to the network operator.

The housekeeping routines for the prototype should be able to measure temperatures at various points, and light sensitive detectors are required to protect the image intensifier electronics. The computer clock has to be updated to a correct time of day.

The station computer should keep various logbooks for imaging, housekeeping and network messages. By using the logbooks, timetables, and the local clock recovery from error situations (such as power failure) should be possible.

Some image post-processing software is also needed. For example, generating keograms is a straightforward process which can be done while compressing the images taken during the night.

4. The station prototype

4.1 Overview

The approach chosen for the all-sky camera station prototype is to use a PC/AT-compatible computer that controls the imaging system. This computer is then connected to a computer network via which remote control can be achieved. Image acquisition is achieved by using a imager that can be mounted inside a special transparent dome. The imager needs not to be in the same building as the station computer. A low light level imaging system that looks very promising for our needs can be purchased as a complete building block from a small US company called *KeoConsultants*.

As the prices of personal computers are constantly falling, a widely used PC/AT-compatible small computer forms a good starting point. Moreover, spare parts can be purchased in almost any computer store that can be found, and there are several millions of users, so their expected lifetime is rather long. In the future more powerful processors will undoubtely replace the current ones, but this will only be of advantage, because more local image processing can be performed.

Another examined possibility is to use "industrial" PC/AT computers, which are more rigid versions of the ordinary models. The current standard for embebbed applications is *PC/104*, in which the motherboards are small and the peripheral cards can be stacked into one pile. They are very suitable for industry conditions, where they have to tolerate humidity, vibration and rough handling. However, these features also mean more expenses, and the conditions at the all-sky camera stations do not require this.

The imaging system manufactured and marketed by KeoConsultants is a complete system consisting of all necessary lenses, a filter wheel, an image intensifier and a CCD camera with control electronics. The company has delivered several tens of these imaging systems to various research groups around the world. The system model for the prototype can detect light intensities above $\sim$ 100R.

An overview of the prototype all-sky camera station is shown in Figure 4.1. The imaging system was borrowed from KeoConsultants to evaluate the imaging performance.

4.2 Optics

The optics consists of a fish-eye lens, an optional filter wheel, an image intensifier, a CCD camera, control electronics and two coupling lenses. For the prototype there

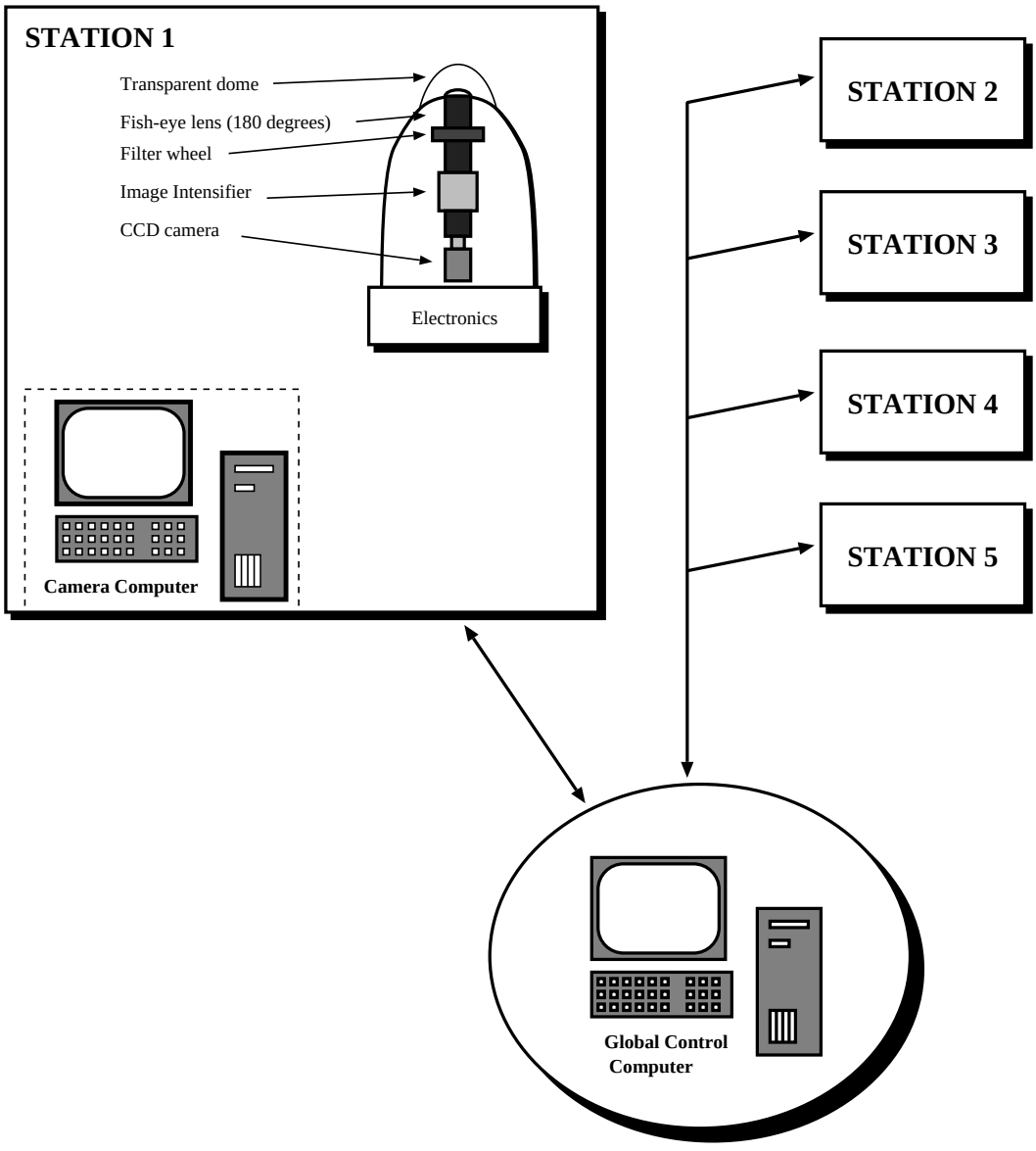

Figure 4.1: Schematic overview of the new all-sky camera station connected to the station network.

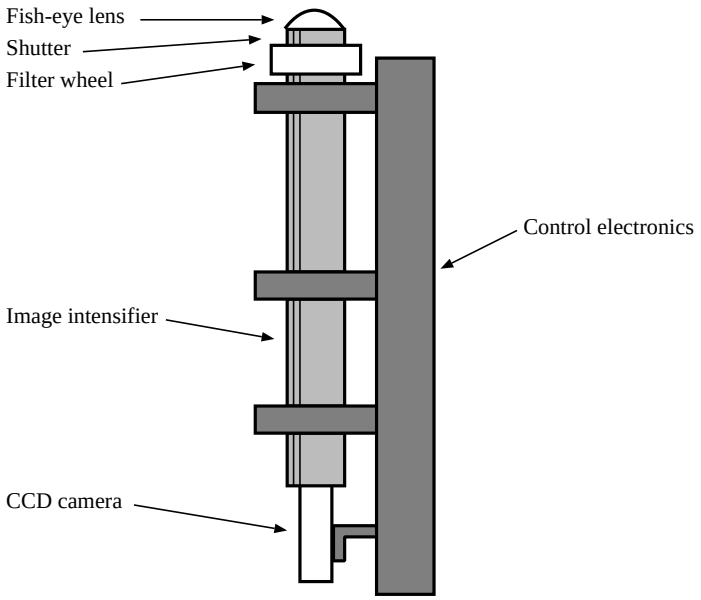

Figure 4.2: Schematic overview of the new all-sky camera.

is only one single filter holder at the moment. The entire configuration is shown in Figure 4.2.

The fish-eye lens has an angular field of view of 180°, so the whole sky can be imaged. Behind the fish-eye lens is an electronically controlled shutter. This shutter protects the image intensifier from too high light intensity that would damage the intensifier.

The filter wheel is placed after the shutter to reduce the effects of the solar radiation. The wheel can accomodate five 3-inch interference filters that have a passband width of 2.0nm. The filter wheel housing is temperature stabilised, because the central wavelength of the passband depends on the filter temperature. The wheel is operated by a DC servo motor, and a filter change takes about 0.25s (ie. change to any filter in the wheel takes less than 0.5s). Further details of the camera can be found in Chapter 6.

4.3 Prototype Housing

No special housing was purchased or built. Instead, the camera frame was attached to temporary test jigs. Preliminary tests with UPS were made.

4.4 Computer

4.4.1 Operating system

There are several different operating systems for PC/AT-compatible computers. However, even though almost every operating system can be connected to a network not all of them allow complete remote control without special arrangements.

Table 4.1: The all-sky camera station computer configuration.

Item	**Details**
Processor type and speed	Pentium-75MHz
Memory	16MB
Harddisk	Two 1.2GB harddisks, total 2.4GB
Display	15 inch monitor, resolution up to 1024×768
Mass storage	HP1532A 4—16GB DAT-drive (DDS2)
Frame grabber card	Data Translation DT-55
Data acquisition card	ADCLONE ACL-812PG+
Precision clock	Rockwell MicroTracker LP (GPS receiver)
Network devices	SMC Ultra Ethernet card and Well 2814SAM modem
Power supply	Powera MATRIX 500 On-line UPS
Watchdog	(not yet implemented)

Linux is a completely free reimplementation of the POSIX specification with SYSV and BSD extensions, which means that it is a "unix" environment. It is copyrighted by Linus Torvalds and other contributors, and is freely redistributable under the terms of the GNU Public License. Some key features of Linux are

- Full source code available.
- Relatively small and stabile.
- Multitasking environment, several processes of selectable priority can be executed simultaneously.
- Multiuser operating system; the system operator uses a more priviledged account, and the imaging software uses an ordinary account (ie. imaging software bugs cannot destroy the actual operating system).
- Straightforward network connection to other computers at FMI/GEO.

The low-level routines were programmed in C, and a set of shell scripts is used in system administration. A very promising new language *Erlang* was used in programming the real-time parts of the software [*Armstrong et al., 1993*]. Erlang is a *functional language*, and it is especially suited for programming fault-tolerant concurrent real-time applications, where the response times are of the order of milliseconds. An Erlang programme consists of several modules that can be run concurrently, and modules can be changed even while the system is running.

4.4.2 Computer hardware

The features of the prototype computer are listed in Table 4.1. As can be seen in the table, most of the components are commonly available, and, in reality, the

choice of the processor is not critical; 16MB of RAM is mainly for smooth operation of the graphical user interface and multitasking demands. The amount of required harddisk space is calculated from the approximated amount of uncompressed image data per day. The image data collected to DATs is sent to FMI/GEO for analysis and long-term storage.

The electrical interface to the CCD camera and camera electronics is handled via a frame grabber card and an analog and digital interface card. The Data Translation's DT-55 frame grabber can digitise an image from a video signal with a spatial resolution of 768×512 pixels. The signal is quantised to 8 bits (grey scale), and there are various options for triggering the capture. The data acquisition card ACL-812PG+ manufactured by Adclone has 16 analog inputs, two analog outputs, 16 digital inputs and outputs, and one programmable counter.

Because all the station activities depend on the time of day and because exact imaging times are needed for scientific purposes, a reliable clock is needed in addition to the onboard clock on the computer mother board. For this purpose a global positioning system (GPS) receiver is used. The Rockwell MicroTracker LP GPS receiver can provide a time mark once per second to an accuracy of $\pm 1 \mu$s [3]. The time of day is received via one of the computer's serial ports. In addition to the time of day, more information is also provided, of which the geographical position[4] of the receiver unit and the date are used.

There are two main categories of uninterruptible power supplies (UPS): on-line and off-line. When using an on-line UPS the mains power charges the UPS batteries and the output power to the equipment is driven by the batteries. Thus, the power for the equipment is "clean" without distrubances from other devices. When using an off-line UPS the mains power goes directly to the equipment, and in case of a power failure the power input is switched from the mains to the batteries. The chosen UPS is an on-line UPS with a computer interface, which can be used for detecting power failures to prepare controlled shutdowns.

One important housekeeping function is a "watchdog", which is an external device that will reset the computer if the computer has not sent an "alive" message during a fixed time interval. This time interval has to be long enough for the system to execute a complete reboot with harddisk checks.

[3] When ignoring the effects SA-code (Selective Availability).

[4] The exact locations of old all-sky stations are well known, of course, but in case of a "portable" station it is very useful to be able to measure the location without additional equipment.

5. Station software

5.1 Image acquisition

The most important software function is the image acquisition. This acquisition is autonomous, and the station itself can store several gigabytes of image data. Because the northern night is long and the brightest moment is around the noon, each operational day begins at local noon. First the station executes a self-check in which the hard-disks and general operation are tested. This self-check includes using the GPS receiver to verify the date and the time of day. After this, the imaging timetable is read and the next activities depend on the contents of the timetable. The general overview of the processes involved in image acquisition is shown in Figure 5.1.

The timetable contains information about when the imaging will be started and stopped. For each image the exposure time and the filter selection[5] is read from the timetable. The filename for every image is evaluated according to the station name, a complete date and time, the filter and exposure settings. A planned acquisition consists of several images with varying filters taken as quickly as possible and a pause before next acquisition. A general operational day is shown in Figure 5.2.

An example timetable file and a couple of screenshots of the user interface can be found in Appendix C.

5.2 Image data processing

The frame grabber software automatically includes texts into the image data which is stored in portable greymap format (PGM). A sample image is shown in Figure 5.3. The texts are appended at the bottom of the image and they indicate the time, the date, the station name and geographical location, the filter used and the exposure time. This is the only data processing operation executed in real time.

After the imaging has finished a subset of all images is processed to generate a keogram for the operational day. This keogram is then included into the image data set.

Because the large amount of images taken during one operational day, the image data is compressed before it is stored to a DAT. The DATs are then collected once a week and transported to FMI/GEO. Usually the all-sky images are analysed visually, and using *lossy compression* methods does not significantly reduce image quality. These compression methods can be very effective by reducing the required

[5] This parameter is included into the prototype software, although there is only one filter.

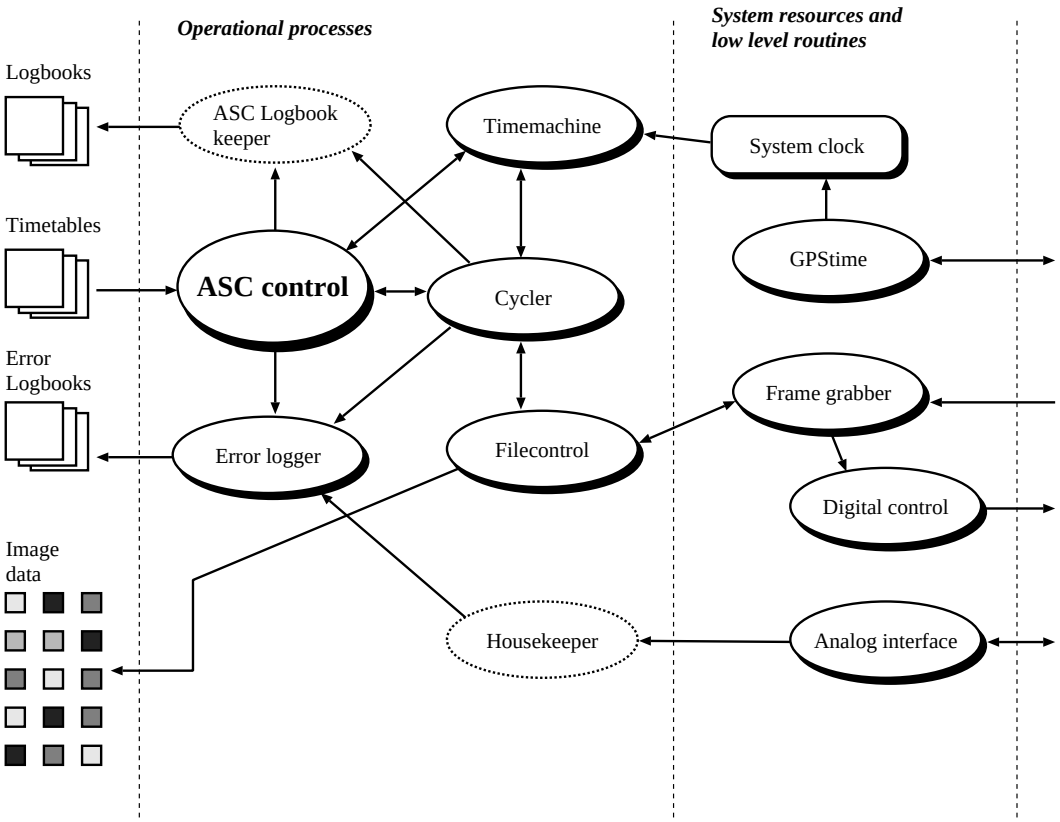

Figure 5.1: Processes involved in the image acquisition; the two dashed processes have not yet been implemented.

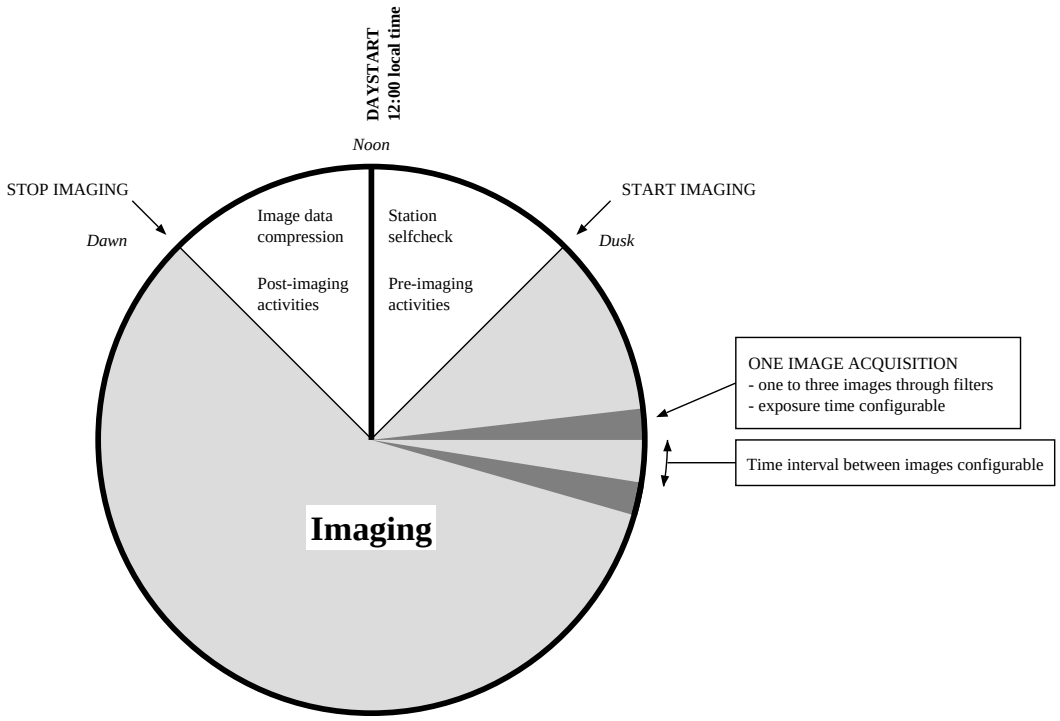

Figure 5.2: One operational day at the all-sky camera station.

storage capacity[6]. However, the effect of the minor errors in the decompressed image can affect results of edge detection or other digital image processing algorithms. By using a *lossless compression* a typical compression ratio is around 1:2 to 1:10 [*Gonzalez et al., 1993*], which is small compression compared to that of lossy compression. It is also possible to take advantage of the time series of the images instead of using separate images.

Because the image processing is of major importance, the effects of different image compression methods must be studied very carefully. In practice, it is very easy to vary the compression method, but classifying the results may be rather complicated and difficult.

5.3 Housekeeping routines

The housekeeping routines take care of the station in general. One key element of housekeeping is to provide a tool for finding software and hardware problems; this is accomplished by keeping various log-books and day-schedule files shown in Table 5.1. The operating system keeps several log-books on its own, and the station software only records its activities separately. Erlang provides one unified error-logger for all Erlang processes, and if a process should terminate unexpectedly, the error-logger will log this.

[6]Visual comparison of old all-sky data between original and compressed and decompressed data indicated little or no difference even with compression ratio of 1:32. The quality of the originals will be better with the new camera, though.

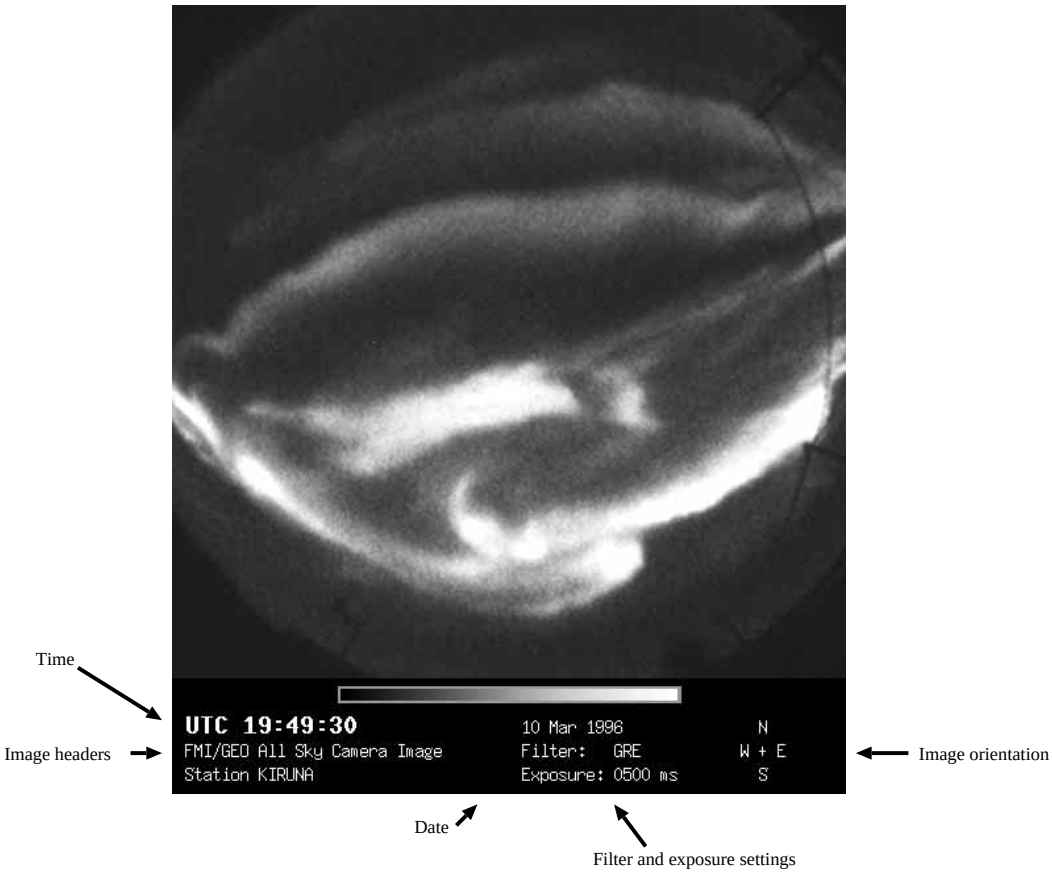

Figure 5.3: An output from the frame grabber software.

Table 5.1: The log-books of the station software. *) Not yet implemented

Log-book name	**Keeper**	**Purpose**
cron	System	Log-book for daily operation controller
messages	System	Various operating system messages
debug	System	Used in debugging operating system resources
syslog	System	General operating system log-book
xferlog	System	FTP transfer log
errorlog	Station	Log-book for error in Erlang processes
dayschedule	Operator	Imaging timetable
ascstatus *)	Station	State transitions; time stamps of imaging start and stop
ascerror *)	Station	Error messages from station software
ascimage *)	Station	Filenames of images that have been successfully stored
ascmail *)	Station	Log-book of sent e-mail
ascstore *)	Station	Filenames of compressed and stored images
hklog *)	Station	Measurements by housekeeping electronics

There are several short shell scripts that are used, for example, in evaluating the status of free hard-disk space, and the operating system provides useful tools for general system maintenance. The log-book "asc-store" holds not only filenames of compressed and stored images but also the compression ratios.

All logged errors are checked once an hour and after the imaging day and then automatically sent to the operator personnel via e-mail. In addition the generated statistics and keograms are sent.

The housekeeping includes the routines needed for keeping the watchdog from resetting the computer. If the computer is reset then the log-books can be used in finding out the reason for malfunction. At the moment the station software will not try to use the log-books and return to the imaging: instead it will stop and leave the situation clean for human investigations.

Because Linux is a multitasking and multiuser operating system, it is possible to remotely monitor and control the station operation. This includes viewing "live" images and inspecting housekeeping measurement results.

5.4 Control Centre Software

5.4.1 Imaging control

One computer at FMI/GEO will be the *all-sky camera network control centre*. This control centre will monitor the operation of all station computers and collect all

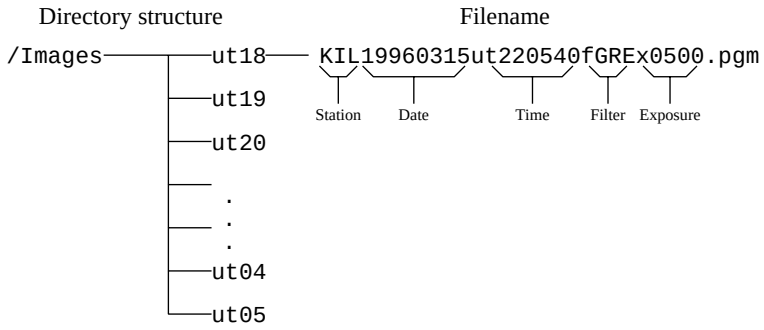

Figure 5.4: The directory structure and filename conventions.

received messages and images for human inspections.

Usually the network can be left operating autonomously, because image acquisition is performed similarly every night during the winter. However, in case of special observation campaigns it will be of advatage to be able to start and stop individual ASC stations, and change imaging parameters.

5.4.2 Image data handling

The prototype station software stores the images into one master directory which contains separate subdirectories for every hour. Each image name has a constant length and is generated from the station name, date, time, the filter used, and the exposure time. Also, the image itself contains the previously mentioned image parameters (see Fig. 5.3). The directory structure and the naming convention is illustrated in Fig. 5.4. The master directory name is changed to the corresponding (start) day when images from a longer period are collected onto a CD-R.

To assist auroral arc movement studies the image can be projected onto a (geographical) map. Also, images from all stations can be used to create a map that covers a larger area.

A short routine was written to project an all-sky image onto a map (see Appendix A). Two parameters are required for the projection: the centre of the image (ie. the image of zenith) and the edge of the image (ie. the horizon). To test the functionality of the routine a comparison test against previously written projection routine was performed. The input for both routines is shown in Fig. 5.5, where the image centre is marked with a small circle and the horizon with a larger circle.

When using the previously written routine, the user follows the auroral arc edges with the mouse cursor and creates a set of edge points whose geographical coordinates are then output. Using these coordinates a polygon is drawn on top of the map that is generated by the newer projection routine, and the result can be seen in Fig. 5.6. The advantage with this new routine is that the map projections can be generated automatically and the whole image can be seen on the map.

The ultimate goal of image handling is automatic recognition of auroral forms and rejection of cloudy or otherwise useless images. For example, instead of projecting the whole image onto a map, only the actual aurorae could be projected.

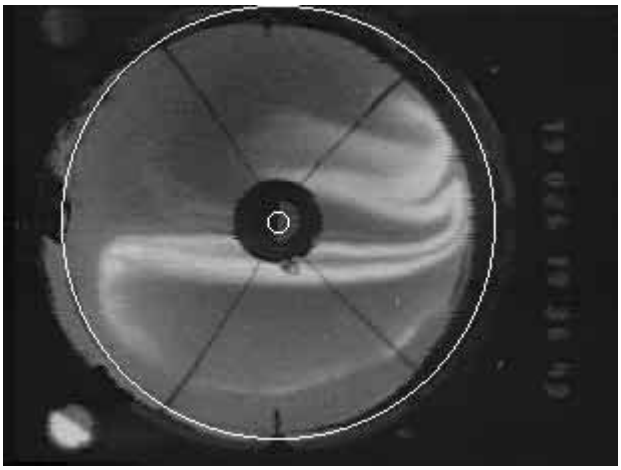

Figure 5.5: The input image: smaller circle is the centre and larger one is (approximately) the horizon.

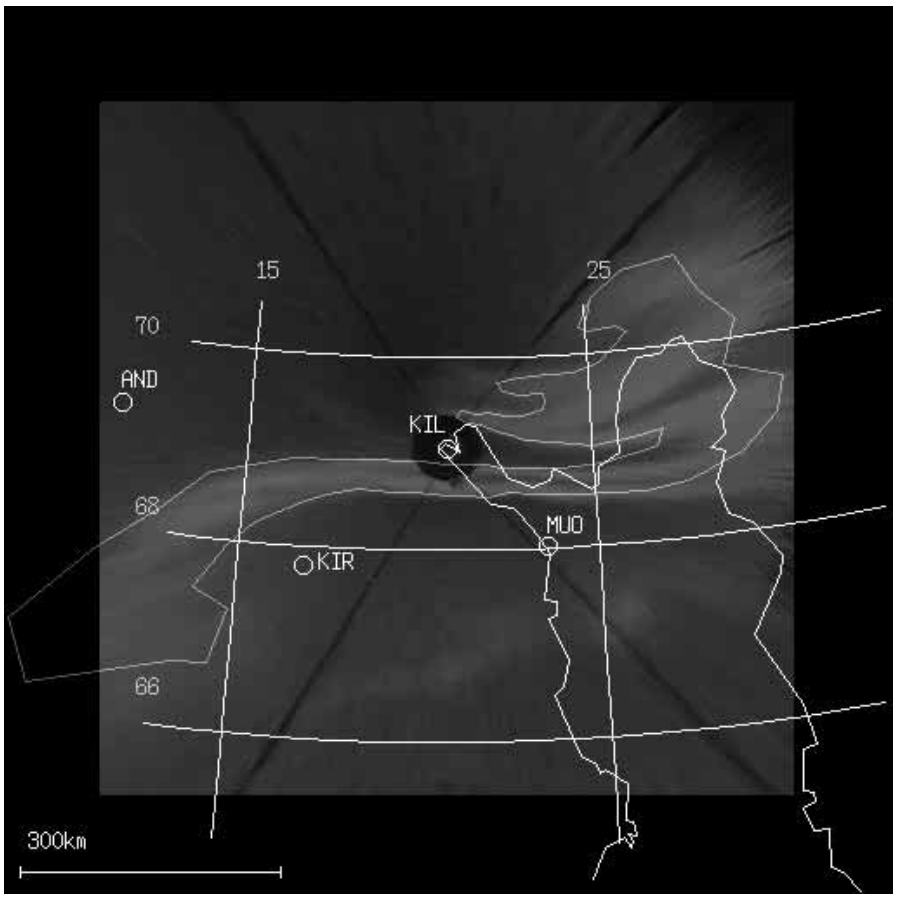

Figure 5.6: The output image: the continuous edge polygon is the output of the old routine and is drawn on top of the output of the new routine.

6. The imager

6.1 Overview

The main function of an ASC is to acquire images of the whole sky. This is accomplished with a set of lenses and imaging elements. The prototype ASC described in this work uses a commercial all-sky camera manufactured by *KeoConsultants*. In the imager there is a fish-eye lens including additional lenses to make the first stage of the image forming telecentric in order to enable the use of narrow bandpass filters. This telecentricity is of major concern because the shift of transmission wavelength with filter angle increases as the angle squared, so that larger ray angles rapidly require much wider filters.

The fish-eye lens, the shutter, the single filter, and the image intensifier form the first stage of the image acquisition. The second and last stage of the optical system consists of a CCD camera and relay optics, which couple the image output of the intensifier to the CCD. Details of the optics can be found in *Eather et al.*[*1993*], and the essential terminology used in describing the optics is explained in Appendix B.

Section 6.3 describes the methods used to control the electrical operation of the ASC. This includes opening and closing the shutter and using full frame integration operation of the CCD camera to vary the exposure time.

6.2 Optics

6.2.1 Fish-eye lens

The fish-eye lens *Canon FD 15mm/F2.8* uses an *equidistant projection* to image the half-space onto the image plane. Let the incident angle of an infinite object be Ψ. Now the distance (in the image plane) d between the image point and the optical axis is

$$d = f\Psi, \tag{6.1}$$

where f is the focal length of the fish-eye lens. Because of the linear relation between d and Ψ this projection is preferred for measurements of zenith and azimuth angles. The fish-eye lens has a field of view of 180°, and the image of horizon is projected furthest away from the image centre and the whole image is circular.

The exit ray cones from the commercial fish-eye lens are made telecentric by adding lenses near the image plane. In telecentric systems the principal ray of all image-forming cones across the field of view crosses the image plane parallel to the

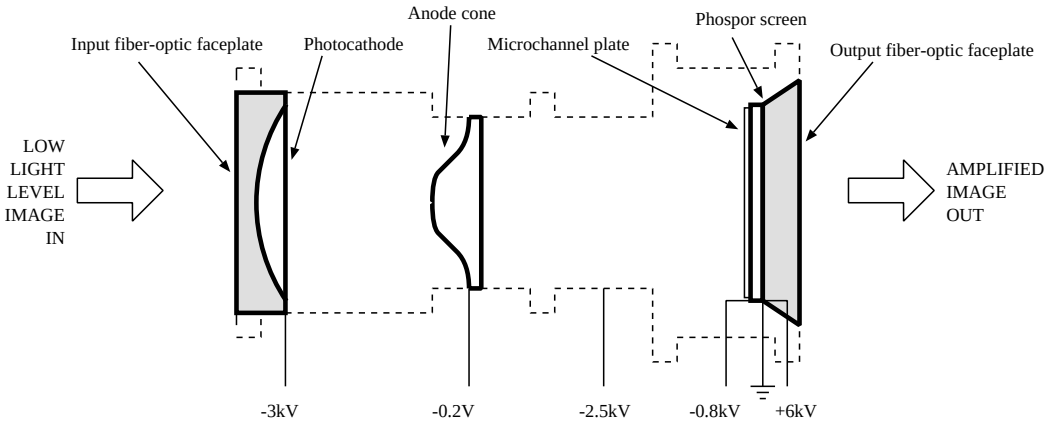

Figure 6.1: The image intensifier

optical axis. The additional lenses have to be chosen in accordance to the model of the fish-eye lens used.

6.2.2 Shutter and filter wheel

The shutter protects the filter and the image intensifier from direct sunlight. The shutter is opened slightly before starting the exposure and closed after the frame grabber has acquired an image. KeoConsultants have had reliability problems with the *Melles Griot* shutter used in the prototype, and this shutter will be replaced with another more reliable shutter in the operational version.

The prototype had a single filter holder. The filter used is a 2-inch narrow-bandpass interference filter. For proper operation of the filter telecentricity is required, because the centre wavelength of the bandpass varies greatly as a function of the incident angles of the incoming rays. The single filter holder will be replaced with an electrically operated filter wheel, which can accommodate five filters. The centre wavelengths that will be used are 427.8nm, 557.7nm and 630.0nm, and the bandpass width is approximately 2nm (-3dB). The filter wheel is also temperature controlled in order to maintain constant wavelength transmission through the filters.

6.2.3 Image intensifier

The relatively high F number image at the filter is re-imaged to a lower F number image at the image intensifier. The intensifier used is a *25mm Microchannel Inverter Intensifier model 3603* manufactured by *VARO* (USA). A schematic overview of the intensifier's inner details is shown in Fig. 6.1.

The low light level image is transmitted to the photo cathode where the photon image is converted into an electronic one. The electrons are accelerated towards the phosphor screen, and the electron amplification is provided by the Microchannel plate. The cathode is thinned tri-alkali for improved blue quantum efficiency, and the output phosphor is P20 for good time response (decay time to the 10% level is $\sim 1 - 2$ms).

6.2.4 CCD camera

The output image from the image intensifier is optically coupled to the *Pulnix TM-765E* CCD camera. A specially designed collimator lens before the camera lens is used to enable the use of an "ordinary" *Nikon 35mm/F1.2* lens with minimal vignetting. The camera outputs a standard *CCIR* video signal (black and white).

The camera in the prototype was not a cooled one, which results in increased noise in the final image caused by thermal noise in the camera. Usable exposure times are usually less than one second, but — according to KeoConsultants — an exposure of 0.5 seconds is sufficient for the required 100R to 10kR operation range.

6.3 Controlling the all-sky camera

The prototype camera requires 110V mains power and a 220V → 110V voltage converter. This power is used by the image intensifier and the shutter electronics. The Pulnix camera uses a separate power supply (220V).

The data acquisition card in the station computer was used to control the shutter and the integration time of the CCD camera. A small external electronics block was built where the all-sky camera electronics, data acquisition card and the frame grabber were connected. The shutter control is independent of the integration time, which enables one to open the shutter before the actual exposure is started. There is a separate switch that can be used to completely disable the shutter operation manually (to protect the shutter during software development). The integration is controlled by using a separate control pin in the camera connector; the power line to the camera uses the same connector and a small cable modification was necessary.

A frame grabber program was written to be able to use the grabber in Linux[7]. The program also controls the shutter. The grabber is first initialised and prepared for acquisition by setting the card's look-up tables and control bits properly. During the integration the signal process in the CCD camera keeps optical black levels resulting in decreased noise during the integration period. The integrated image is the first full frame output (ie. two fields) by the camera after the integration signal is rejected, and this rejection also triggers the frame grabber. The schematics of the electronics block is shown in Fig. 6.2.

The integration time is handled by a Unix system call *usleep* which suspends execution of the calling process for a given number of microseconds. This is sufficiently accurate for evaluating the performance of the prototype, and a complete KeoConsultants camera uses special circuitry to generate precise integration times.

6.4 Corrections and calibration

6.4.1 Dark current and read-out noise

Thermal noise in the imaging elements creates *dark current*. This dark current can easily be measured by acquiring images when the shutter is closed. These *dark frames* are then subtracted from the image to get the actual image caused by the

[7] Usually PC/AT computer peripheral manufacturers provide drivers only for DOS and Windows

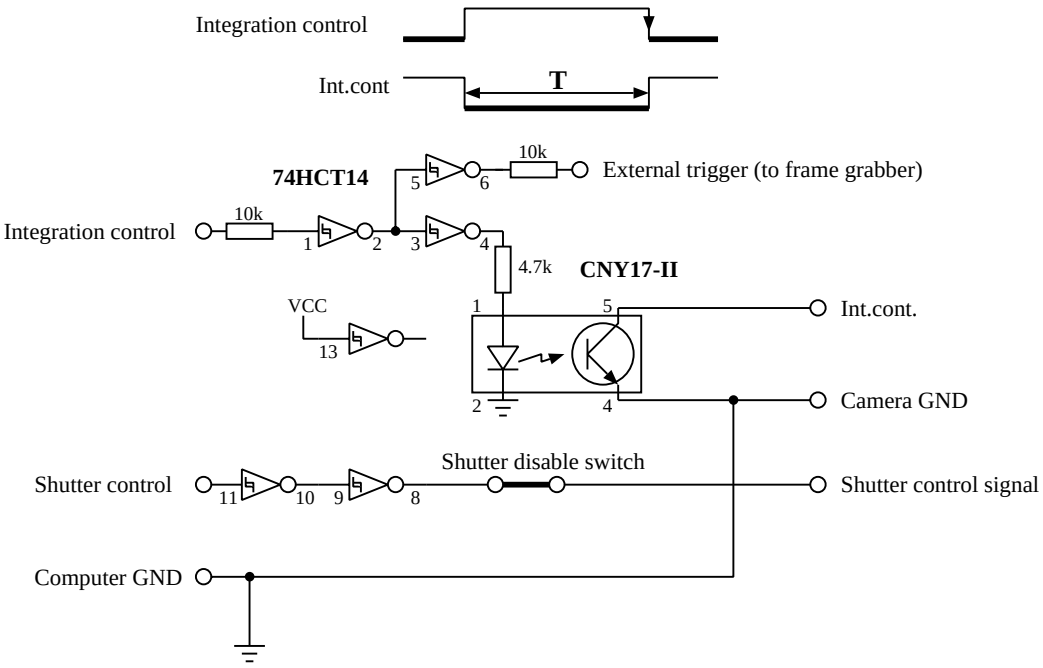

Figure 6.2: The external electronics block

object. To minimise dark current the sensor chip can be cooled with e.g. Peltier coolers. The sensor is usually kept at constant temperature to minimise effects due to environmental changes. Both the image intensifier and the CCD camera create dark current in the ASC. Acquisition of dark frames is easily accomplished; the software is configured to acquire images with a closed shutter at specific intervals.

When reading the image from a CCD the sensor electronics cause *readout noise*. This readout noise limits the detection of weak signals; if the signal level is of the order of the readout noise, the signal cannot be detected. In addition to the sensor readout noise the frame grabber also adds noise, and in more expensive CCD cameras the pixel readings are digitised in the camera and images are transferred digitally.

6.4.2 Flat-field correction

To correct the non-uniformities in the imaging system a *flat-field correction* is performed. Ideally a uniformally illuminated surface is measured and using this *flat-field frame* the non-uniformities in the optics and sensor pixels can be corrected. Flat-field correction is crucial for photometry, and any change in the optics — be it temperature or shadows of dust particles on the filter — affects the flat-field. It should be remembered that the dark current also affects the flat-field frame, and thus the dark frame has to be subtracted from the flat-field before performing the correction. The non-uniformities in the imaging system are not random; in theory, a new flat-field frame needs to be generated only when something is changed in the system.

Performing a proper flat-field correction with the ASC is not a straightforward task: the FOV of the camera is 180° and creating a uniform illumination over the

whole FOV is difficult. It would also be preferable to acquire at least one flat-field frame per imaging session. Astronomers usually aim their instruments at a reasonably evenly illuminated spot in the evening sky. Perhaps, a set of suitably "quiet" all-sky images can be used to calculate a flat-field frame for each night. Flat-field correction clearly requires more detailed studies.

6.4.3 Geometrical alignment and calibration

All-sky cameras should be aligned to magnetic north-south direction for easy interpretation of auroral arc movements. Also the centre of the image should be pointing to the zenith. To find the correspondence of the image points and the object points (assuming a known altitude) the camera has to be calibrated.

Very likely the error in estimating the altitude from which the emission comes is greater than that of the aberration errors in the optics. However, the north-south alignment can be measured by imaging (known) stars, after which an image rotation matrix can be generated.

6.4.4 Brightness calibration

To be able to measure aurorae in absolute units the response of the system has to be calibrated against known light standards. A method used by KeoConsultants is to use a larger calibration setup before the start of every imaging session and use a smaller portable light standard to check the calibration in field. Another possibility is to use stars with known brightness magnitudes.

Previous all-sky cameras used by FMI had small radioactive light standards next to the spherical mirror, and each image then contained a couple of known brightnesses. This could also be arranged with the new cameras; the practical FOV is around 160° and small reference light sources could be placed at low elevation angles where the surrounding objects restrict sky visibility.

7. Test results

7.1 Laboratory tests at FMI/GEO

After a successful operation system installation and configuration the station computer system was tested by using it as an ordinary workstation at FMI/GEO. This included "remote" operation via network. Operation of the DAT drive was tested by making backups and comparing the data written to the tape to the data residing on disk. An indexing programme *dds2tar* was tested; by using *dds2tar* one can create an index file which contains the names of the data files with their corresponding tape block numbers[8]. The block number can then be used to wind or rewind the tape quickly to the correct position, which considerably speeds to search-and-read process.

A video tape recorder was used as a video signal source before the CCD camera was available; preliminary tests of the image acquisition routine were performed by acquiring images every 20 seconds. During the first tests with the CCD camera disturbing "stripes" in the image were noticed: these stripes disappeared after the mains plugs were connected to the same mains outlet. The integration feature of the CCD camera was tested by imaging stars. By using exposure times around 2s one was able to detect stars that could not be visually seen due to the city lights. A fine image of *Orion Nebula* and some of the surrounding stars (magnitudes from star cataloques were up to 7–8) was captured.

7.2 Hankasalmi 14.–18.2.1996

The prototype ASC was transported to Hankasalmi 350km north of Helsinki for a short field test. The background illumination due to city lights is considerably lower in Hankasalmi than in Helsinki, and testing autonomous operation in a realistic environment was possible.

There is a small tower on top of which there is a transparent dome with a diameter of approximately two meters. The camera construction was attached to the supporting fixture as shown in Fig. 7.1. To minimise reflections from artificial light sources all nearby building lights were shut off and the computer LEDs inside the dome were taped with opaque tape.

Although three nights of four were completely cloudy, the fourth night was clear and sensible imaging was possible. Three exposure times were used (500ms, 800ms

[8] In DDS2 systems one tape track contains a running block number.

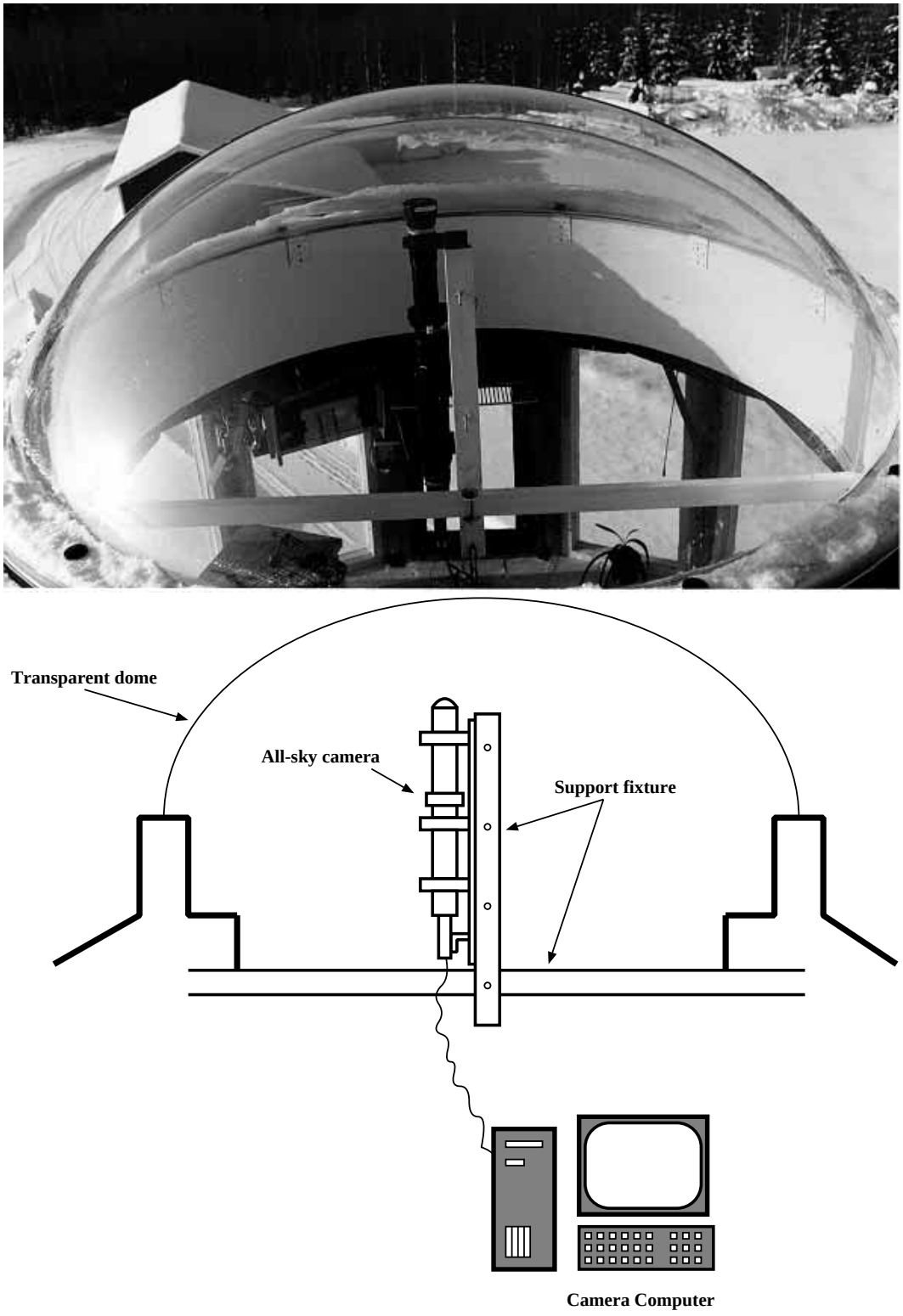

Figure 7.1: The dome in Hankasalmi.

and 1500ms) and the intensifier gain was kept at approximately 75% of maximum gain. A total of 523 images were acquired.

In addition to all-sky images, a set of dark images were captured to investigate dark current and read-out noise. During the exposure of the dark images the shutter was closed and the lens cap was also on. The average pixel intensity of the dark images was 28 out of 255 with an exposure of 800ms. In order to decrease the dark count a separate video amplifier with variable gain and offset may be required. More expensive frame grabbers usually include circuitry needed for this video signal preprocessing already onboard.

In Hankasalmi the ASC successfully imaged three nights autonomously. An operator was needed only for setting the initial imaging parameters. Some experiments were performed manually by using different exposure times and intensifier gains. Also, during the first hours of the clear night a filter (557.7nm) was inserted in the light path. Then the filter was removed and autonomous operation was started.

7.3 Tests in Kiruna 3.–14.3.1996

7.3.1 Test set-up

Because no aurorae were observed in Hankasalmi it was considered necessary to have another field test period. Swedish Institute of Space Physics (IRF, Institut för Rymdfysik) in Kiruna kindly provided one of their all-sky observation domes at FMI's disposal. The domes at IRF are somewhat smaller than the one in Hankasalmi, and they suit considerably better for optical measurements.

The test set-up was similar to Hankasalmi: the camera placed in the middle of the dome, and the station computer was below the camera. A couple of extension cables were necessary, because the distance between the computer and the camera was greater than it was in Hankasalmi.

7.3.2 Operating the prototype

The prototype station made observations every night during the 12-day stay in Kiruna —the total number of acquired images exceeds 15000. The station operation was started manually in the afternoon and the actual imaging started and stopped successfully at pre-defined times.

7.3.3 Performance measurements

Dark images

The dark image results from Hankasalmi needed further investigations to find out, whether the cause of the average background of 28 digital units noticed in Hankasalmi is caused by dark current or whether there is bias in the digitising. This time several exposure times between 100ms and 2.4s were used, and each dark image was an average of five images. Again, the shutter was closed and the lens cap on to minimise background illuminations. The measurement plot is shown in Fig. 7.2.

One of the measurement sets was done at daytime when the Sun was warming the camera; the increase in the temperature increases the thermal noise and thus

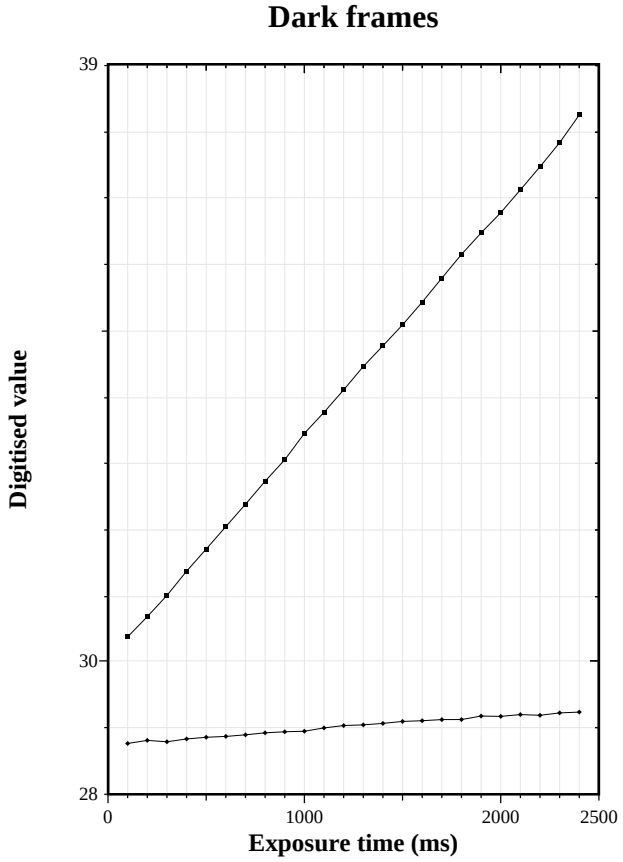

Figure 7.2: Dark image measurements; upper line = camera heated by the Sun, lower line = cooler camera.

dark current. As one can clearly see there is some biasing in the digitised values, because doubling the exposure time does not double the average background value.

A straight line was fitted to the measurement results by using least-mean-square (LMS) criteria, and the bias and dark count were estimated to be

$$\begin{aligned} \widehat{C}_{M,warm} &= 30.0\text{bits} \\ \widehat{C}_{M,cool} &= 28.8\text{bits} \\ \widehat{C}_{D,warm} &= 3.40\text{bits/s} \\ \widehat{C}_{D,cool} &= 0.21\text{bits/s}. \end{aligned}$$

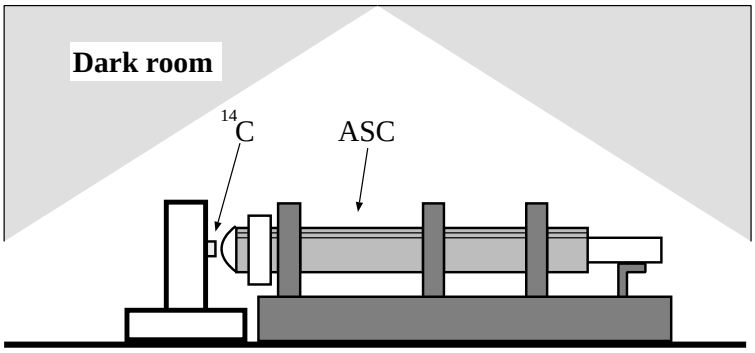

Figure 7.3: Calibration configuration.

Initial calibration measurements

To measure the sensitivity of the camera a setup shown in Fig. 7.3 was used. The light source uses radioactive ^{14}C to provide a constant emission, and its brightness was given in rayleighs per ångström (R/Å). By multiplying this brightness by the width of the filter the source radiance as seen by the instrument can be obtained. The latest source calibration was performed in August 1985, and thus the brightness $B = 251.0\text{R}/$ is somewhat lower nowadays, the width W of the filter bandwidth is 20, and the source radiance is

$$L_s = BW = 251.0 * 20\text{R} = 5020\text{R} \tag{7.1}$$

The measurement results have not yet been completely analysed, and thus only initial results are shown. Also, because the integration control is not synchronised to the video output the actual integration time differs from its nominal value.

Each CCD image pixel can be mapped to a corresponding area at the filter; the 2 inch (50.8mm) image covers approximately 512 pixels, so the pixel size at the filter is $d = 50.8/512 = 0.0992\text{mm}$. Thus the pixel area (this camera has square pixels) at the filter is

$$a = 9.9 * 10^{-4}\text{cm}^2. \tag{7.2}$$

The focal length of the F3.5 Canon fish-eye lens is 35mm, and it collects light from a half-angle of $\alpha = \tan^{-1}(1/(2F)) = 0.1419\text{rad}$ ($= 8.1°$). The cone solid angle is then

$$\omega = 2\pi(1 - \cos\alpha) = 6.3 * 10^{-2}\text{sr} \tag{7.3}$$

Assuming 70% overall lens transmission, and using the quantum effiency (QE) of the intensifier 12% and the filter transmission of 70%, and assuming that every cathode photoelectron is amplified enough to produce a detectable CCD response [*Eather et al., 1993*], we get the theoretical count rate per pixel for $L = 1\text{R}$ input

$$\begin{aligned} C_{exp}/t &= \eta L a \omega \\ &= 0.059 * \frac{10^6}{4\pi} * 9.9 * 10^{-4} * 6.3 * 10^{-2} \\ &= 0.29 \text{ counts/(pixel s)} \end{aligned} \tag{7.4}$$

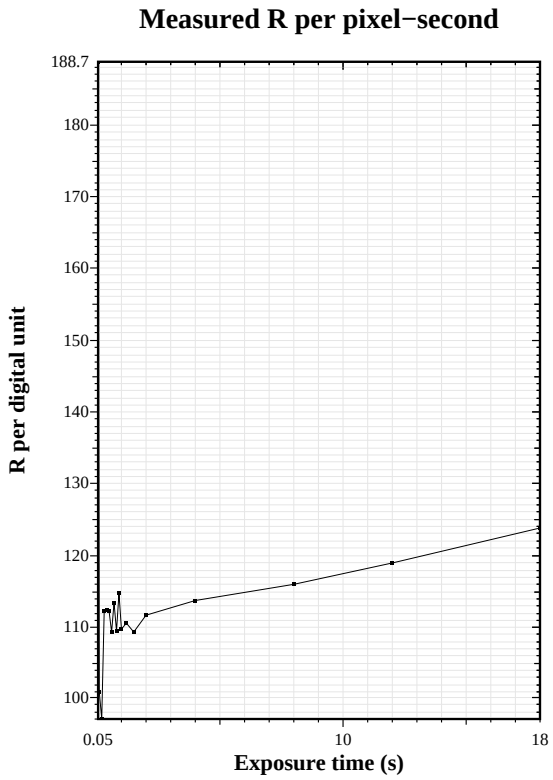

Figure 7.4: Rayleighs per digital unit.

Thus, for every pixel to have 1 event during a one-second exposure the required source radiance is about 3.4R and with the 5020R-source one gets 1450 counts per pixel-second. This counts per second value can be used to find out the sensitivity of the system:

$$\Delta C = \frac{L_s T}{C_S - C_T}, \tag{7.5}$$

where ΔC gives the number of rayleighs described by one count, C_S is the count measured at the source image, and C_T is the total background count including dark current. Both C_S and C_T are average counts inside of an area in the image. The estimated average ΔC is

$$\Delta \widehat{C} \approx 115, \tag{7.6}$$

and the individual measurements are shown in Fig. 7.4.

In theory, if the response of the imager is linear, the curve in Fig. 7.4 should be a horizontal line, because the source radiance was kept constant. When the first attempt to measure a "calibration" image set was performed, the results were even more chaotic; a software bug in the exposure time control subroutine was fixed, and everything was re-measured. It is very likely that the deviation from a straight line is caused by the unexactness of the exposure time. This deviation increases as the

exposure time decreases, and when the timing error is of the order of the exposure time, the expected error in the result naturally increases. Even though the CCD integration control signal is generated by software, the pulse width was surprisingly constant when measured with a digital oscilloscope. More detailed tests have to be performed after the frame grabber and exposure time are properly synchronised.

7.4 Image compression

A selection of auroral images were compressed by using JPEG-compression to test the effect of the errors introduced in decompressed images. It was noticed that small intensity decoding errors due to lossy compression significantly degraded image quality when observing faint aurorae. It is possible that by using different compression settings an acceptable image quality versus compression ratio compromise is found, but further studies are clearly required.

7.5 Auroral observations

During the 12-day stay in Kiruna several auroral events were observed —despite of the minimal Solar activity. During the first few nights the Moon was full, and some blooming effect could be observed. Fortunately the blooming does not prevent auroral observations, and some aurorae were imaged, even though the brightness of the Moon degrades overall contrast.

Two of the most eventful nights were on 9th and 10th of March: the biggest substorm so far this spring was observed. The interval between images was changed to 10 seconds, and a total of around 4500 images were captured during these two nights. The exposure times were purposely varied to investigate the sensitivity of the imager. Figure 7.5 shows a keogram generated from 70 images taken at a 10-second interval. A selection of those images is shown in figure 7.6; note the fading effect in the arc just before the whole sky is filled with aurorae.

During quiet sections some experimenting was done: a set of images with equal exposure time but with different intensifier gains, and one set without the 557.7nm-filter were captured. Two nights were imaged in such a way that every 10th image had a longer exposure of 1000ms while others had 500ms-exposure.

In Kiruna there were also two other auroral cameras in operation: ALIS (Auroral Large Imaging System) and an old FMI ASC delivered to Sweden in the 1970's, both operated by IRF. Comparisons between the images of the three cameras will be done later this year —it will be most interesting to compare the old design and the prototype.

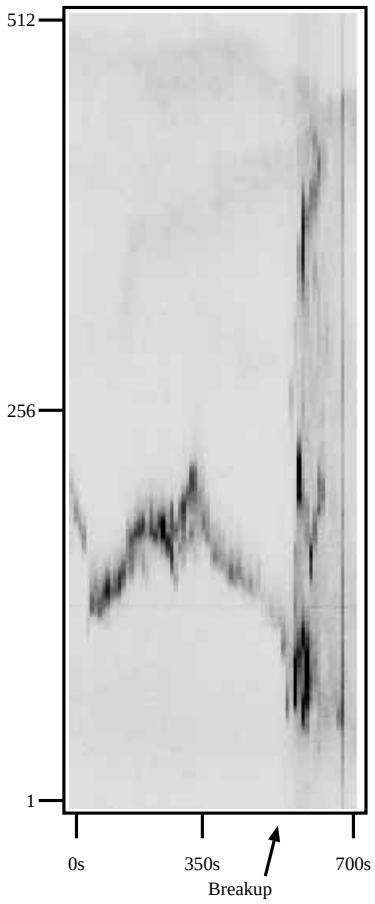

Figure 7.5: A keogram of a breakup in Kiruna. Time interval is 10 seconds, and greyscale is negative.

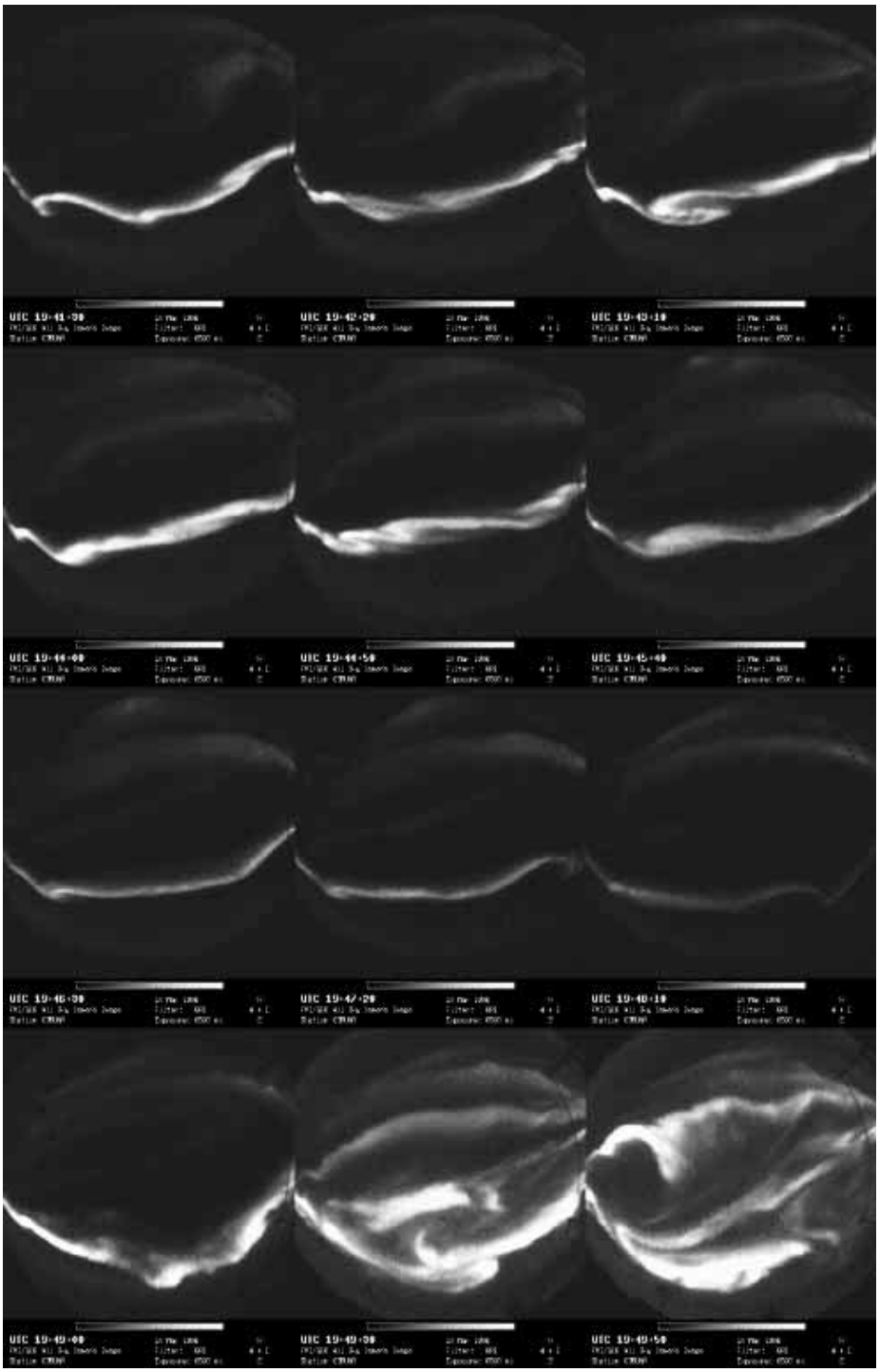

Figure 7.6: The breakup in the keogram in Fig. 7.5 as seen by the all-sky camera.

8. Summary and conclusions

8.1 Prototyping results

In this work a prototype all-sky camera station was built and tested in real operation environment. Much of the station software was written, but the emphasis was on those routines that are required for image acquisition, and thus further software development is necessary.

The operation of the station was first tested at FMI/GEO, and then in Hankasalmi. The test at FMI/GEO indicated that the station computer was functioning properly, and the software was ready for image acquisition. In Hankasalmi the prototype station operated autonomously four nights, imaged stars, and indicated that in the following tests one could concentrate on imaging performance instead of operation tests.

The latest tests in Kiruna proved that the prototype can operate autonomously and image auroral events successfully. At the current stage of software development a human operator is needed to start the imaging, however. The quality of images was found satisfactory for auroral arc and form studies, and by using simple fundamental image processing techniques —such as histogram equalisation— also fainter diffuse aurorae could be recovered from the seemingly dark raw images.

The preliminary calibration results indicate that the imager meets the requirements set for sensitivity, which confirms the conclusions from visual examination of the auroral images. The calibration experiments and the dark frame measurements also indicate that proper system setup is required: the integration control has to be synchronised to the video signal, and the bias in digitising needs correction to be able to fully exploit the whole 8-bits resolution. There will be further development before the next imaging season.

8.2 Further development

The prototype design appears to be successful: the camera construction manufactured by *KeoConsultants* suits well the needs, and the station computer system is capable of acquiring auroral images. There are, however, some details that require further studies, experiments and improvements:

- station housing; suitable housing needs to be manufactured in order to start operation in winter -96–97.

- frame grabber bias; the bias in the video signal has to be adjusted to maximise the dynamic range of image digitising,
- frame grabber synchronisation; due to the deviation of exposure time, unnecessary measurement errors are produced.
- the relay lens positions require adjustment; as seen in the images the edges of the circular image were clipped. This can be corrected by re-positioning lenses between the image intensifier and the CCD camera.
- complete calibration; the sensitivity and linearity of the imager should be measured by performing a thorough calibration. This also includes developing a suitable practice for flat-fielding and calibrating the imager. This practice should be simple enough to perform flat-fielding more or less automatically without bringing the imager into a laboratory.
- software development; most of the network operation software including the network control centre software has not yet been written. Tools for effortless image searching and displaying would also be most useful for effective scientific studies.

The most important item in the previous list is undoubtedly the station housing. Almost all of the other items are not essential for operation but only improvements to the design; it is possible to study the forms and movements of auroral arcs by using the current hardware and software configuration.

8.3 Decisions

The space plasma physics group at FMI/GEO decided to order three similar imagers from *KeoConsultants*. These imagers will be equipped with filter wheel and complete control electronics that will generate exact exposure times. The prototype that was partly borrowed will be completely purchased to be able to develop software. The components of the prototype will also be used as spare parts.

A network of three digital cameras will be stationed during the fall of 1996 to allow full scientific measurements during the season 1996–1997.

References

[*Armstrong et al., 1993*] Armstrong Joe, Virding Robert, Mike Williams, "Concurrent programming in Erlang",Hertfordshire, Prentice Hall International, 281 pages.

[*Baker et al., 1989*] Baker K. B., and S. Wing, 1989, "A new magnetic coordinate system at high latitudes",In:*Journal of Geophysical Research*, Vol. 94, pp. 9139–9143.

[*Carlson et al., 1995*] Carlson H.C., and Egeland A. "The aurora and the auroral ionosphere", In: Kivelson M.G., and Russell C.T. (ed.), "Introduction to space physics", University of California, Los Angeles, Cambridge University Press, pp. 459–500.

[*Eather et al., 1993*] Eather Robert H., Lance Cyril, 1993, "High Frequency Active Auroral Research Program (HAARP) IMAGER", PL-TR-93-2219, Brookline, KeoConsultants, 309 pages.

[*Gonzalez et al., 1993*] Gonzales Rafael C., Woods Richard E., 1993, "Digital image processing", Reprinted with corrections 1993, University of Tennesee, Perceptics Corporation, Addison-Wesley, 716 pages.

[*Hecht, 1987*] Eugene Hecht, 1987, "Optics",Second edition, Adelphi University, Addison-Wesley, 676 pages.

[*Huffman, 1992*] Robert E. Huffman, 1992, "Atmospheric Ultraviolet Remote Sensing",Phillips Laboratory,Massachusetts, Academic Press, pp. 21–34.

[*Hunten et al., 1956*] Hunten D.M., Roach F.E., Chamberlain J.W., 1956, "A photometric unit for the airglow and aurora",In: *Journal of Atmospheric and Terrestial Physics*, Vol. 8, pp. 345–346.

[*Jokela, 1992*] Kari Jokela, 1992, "Radiometrian perusteet ja optisen steilyn mittaukset",Espoo, Otatieto, 47 pages.

[*Jain, 1989*] Jain Anil K., 1989, "Fundamentals of Digital Image Processing", University of California, Davis, Prentice-Hall, New Jersey, 569 pages.

[*Karttunen et al., 1995*] Karttunen H., Donner K.J., Kröger P., Oja H., Poutanen M., 1995, "Thtitieteen perusteet", URSA, renewed edition, Ykkös-Offset, Vaasa, 656 pages.

[*KeoConsultants, 1993*] Anon., 1993, "Telecentric lens systems for widefield low-F# monochromatic imaging", Massachusetts, KeoConsultants, 24 pages.

[*Kernighan et al., 1988a*] Kernighan Brian W., Ritchie Dennis M., 1988, "The C programming language",Second edition, AT&T Bell laboratories, New Jersey, Prentice Hall, 272 pages.

[*Kernighan et al., 1988b*] Kernighan Brian W., Pike Rob, 1988, "The UNIX programming environment", Bell laboratories, New Jersey, Prentice Hall, 357 pages.

[*McPherron, 1991*] McPherron, R. L., 1991, "Physical processes producing magnetospheric substorms and magnetic storms", In: *Geomagnetism*, Vol. 4, p. 593, Academic Press, San Diego, CA.

[*Parks, 1991*] Parks, George K., 1991, "Physics of Space Plasmas, an introduction", University of Washington, Seattle, Washington, Addison-Wesley, pp. 1–18.

[*Pellinen et al., 1995*] Pellinen, R. J., T. I. Pulkkinen, A. Huuskonen, and K.-H. Glassmeier, 1995, "On the dynamical development of the downward field-aligned current", In: "The sub storm current wedge", *Journal of Geophysical Research*, 100, 14863.

[*Pellinen et al., 1996*] Pellinen R.J., Pulkkinen T.I., Kauristie K., Syrjsuo M., "Use of ground-based imaging networks in studies of magnetospheric dynamics", Second International workshop for the coordination of ground-based observations and Cluster, submitted, 1996.

Appendix A

Projecting an image onto a map

A.1 Map projection

There are a great number of different map projections. Because it is impossible to project a sphere onto a plane, every projection introduces distortion. Different projections are used to minimise the projection error in some specific sense, such as correct distances or areas.

In this work we use a plane projection. We select the location of the centre of the map and place a tangent plane at that point on the sphere. Each point on the sphere is then projected onto this plane parallel to the direction of the plane normal vector at the centre point. The principle is illustrated in Figure A.1. A plane projected map is very accurate near the tangent point, and the angles measured from this point are correct.

The vector $\mathbf{r}(\theta, \varphi)$ points from the centre of the Earth to the point to be projected onto the map. θ and φ are the latitude and the longitude of the point. The length of $\mathbf{r}$ is $R = |\mathbf{r}| = R_e + h$, where R_e is the radius of the Earth and h is the altitude of the point.

Now, the x-, y-, and z-components are respectively

$$\mathbf{r}(\theta, \varphi) = R\left(\cos\theta\cos\varphi\ \mathbf{i} + \cos\theta\sin\varphi\ \mathbf{j} + \sin\theta\ \mathbf{k}\right). \tag{A.1}$$

To form the unit vectors for the tangent plane at $\mathbf{r}(\theta, \varphi)$ we differentiate the components

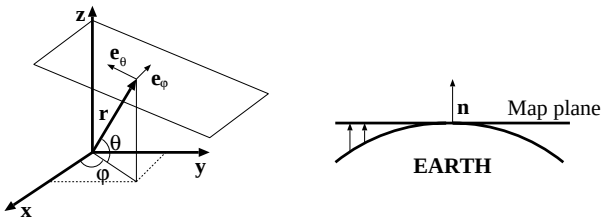

a) placing the map plane b) projecting the map points

Figure A.1: The principle of projection

$$\frac{\partial \mathbf{r}}{\partial \theta} = R(-\sin\theta\cos\varphi, -\sin\theta\sin\varphi, \cos\theta), \tag{A.2}$$

$$\frac{\partial \mathbf{r}}{\partial \varphi} = R(-\cos\theta\sin\varphi, \cos\theta\cos\varphi, 0), \tag{A.3}$$

and then divide each component by its length:

$$\mathbf{e}_\theta = (-\sin\theta\cos\varphi, -\sin\theta\sin\varphi, \cos\theta) \tag{A.4}$$

$$\mathbf{e}_\varphi = \frac{1}{|\cos\theta|}(-\cos\theta\sin\varphi, \cos\theta\cos\varphi, 0). \tag{A.5}$$

Given the tangent point $\mathbf{r_0} = \mathbf{r}(\theta_0, \varphi_0)$ we use (A.5) and (A.5) to fix the unit vectors that form the map plane: $\mathbf{u_x} = \mathbf{e}_\theta(\theta_0, \varphi_0)$ and $\mathbf{u_y} = \mathbf{e}_\varphi(\theta_0, \varphi_0)$. Note that $\mathbf{u_x}$ points to the north and $\mathbf{u_y}$ to the east.

Then for the given point $\mathbf{r}(\theta, \varphi)$ to be projected onto the plane, the x and y coordinates are:

$$\begin{cases} X = (\mathbf{r} - \mathbf{r_0}) \cdot \mathbf{u_x} \\ Y = (\mathbf{r} - \mathbf{r_0}) \cdot \mathbf{u_y} \end{cases} \tag{A.6}$$

A.2 Finding corresponding points in the image and on the map

The fish-eye lens used in the all-sky camera uses a so called *equidistant projection* to image the half-space onto the image plane. If the angle between the incoming ray and the optical axis of the system is Ψ, then the distance d between the image point and the axis is

$$d = f\Psi, \tag{A.7}$$

where f is the focal length of the fish-eye lens.

In two-dimensional situation we naturally have to know the direction of the incoming ray in order to be able to find the correct image point by using circular coordinates (d, ϕ). If we can assume that the light source is at an altitude of h we have a situation where we can calculate the necessary angles (Figure A.2).

To project the image onto a map we can either project each of the image pixels to the desired height and fill the area corresponding to the image point with its intensity, or we can project a selected map point to the image plane and find out the corresponding image point intensity. The latter method was chosen, mainly because it is straightforward to implement and a completely filled map at desired resolution —be it realistic or not— is always produced.

The image data can be considered as a matrix that contains the intensity values for every image pixel. Similarly we can form a map matrix into which the mapped intensities will be placed. In case of colour images we can use tensors in place of the matrices — the third dimension contains the different colour components.

Let the size of the image matrix C be $o \times p$, the radius of the image R_i pixels, and the size of the map matrix M $n \times m$ (Figure A.3).

Now, we use the map projection described previously and place the location of the viewing point (ie. the all-sky camera) at (x_0, y_0) in the map matrix M. Then we let $x \in [-w \dots w]$ and $y \in [-h \dots h]$, where w and h are the half width and the half height of the map matrix. Then for each map point (x, y) we use the distance between the point and the all-sky camera and the projection height to find out the angle Ψ:

$$\Psi = \arctan\left(\frac{\sqrt{(x-x_0)^2 + (y-y_0)^2}}{h}\right) \tag{A.8}$$

and

$$\phi = \arctan\left(\frac{x-x_0}{y-y_0}\right). \tag{A.9}$$

We have to use the signs of $(x - x_0)$ and $(y - y_0)$ to select the correct quadrant to be sure that $\phi \in [0, 2\pi]$.

Now we can use (A.7) to find out the value of d or use the pixel radius R_i and the fact that when $\Psi = \pi$ (ie. the incoming ray is horisontal), the distance between

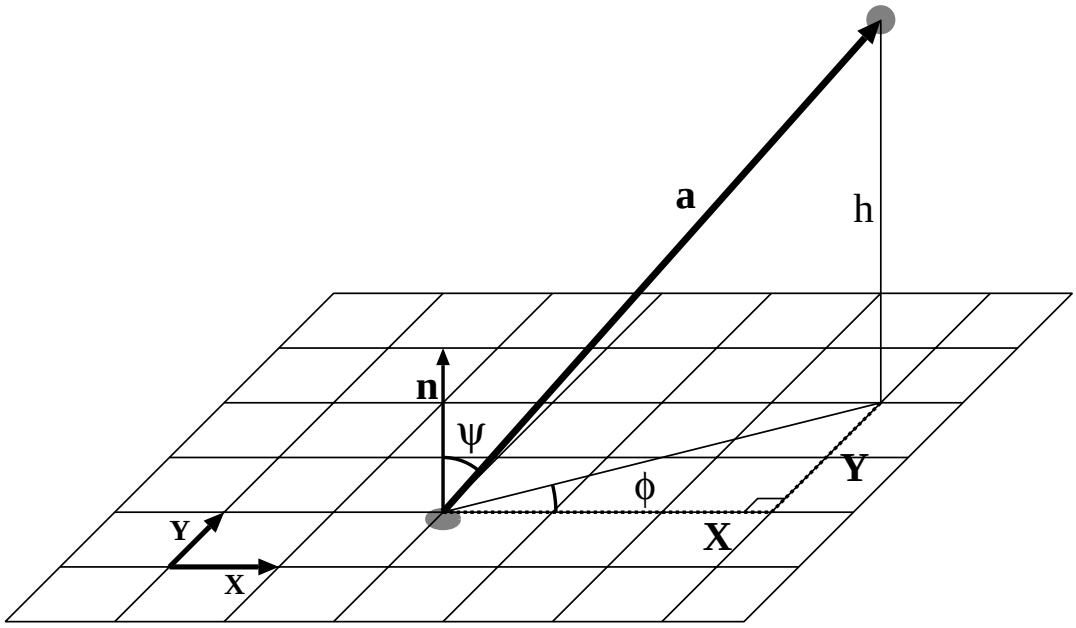

Figure A.2: Finding corresponding points

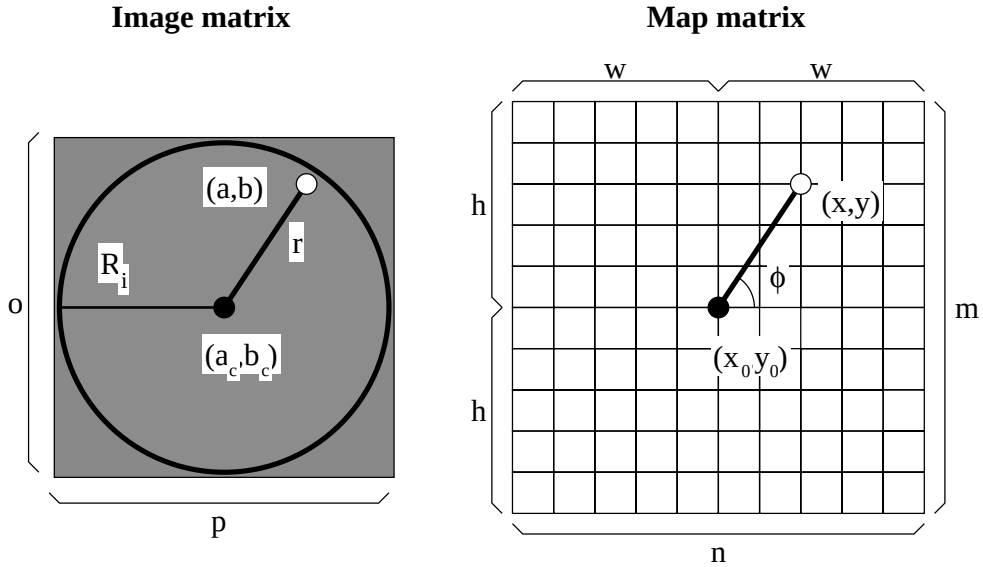

Figure A.3: The image and the map matrices

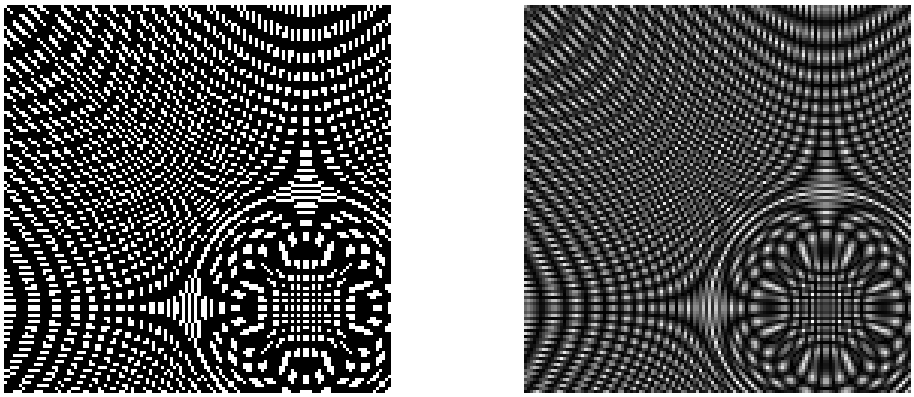

Figure A.4: Generated map projections, without interpolation on the left and with interpolation on the right. The centre of the map is inside the circular formation in the lower right corner.

the image point and the centre of the image is exatly R_i to form an equation for the distance. Let D be the distance from (a_c, b_c) to (a, b) in pixels (see Figure A.3):

$$D = \frac{2\Psi R_i}{\pi}. \tag{A.10}$$

With this information we get the pixel coordinates

$$\begin{cases} a &= a_c + D\cos\phi \\ b &= b_c + D\sin\phi \end{cases} \tag{A.11}$$

The intensity value in $C(a, b)$ is then copied to the corresponding point $M(x_0 + x, y_0 + y)$ in the map matrix.

One can use interpolation when (a, b) is not an integer point to generate a smoother image. However, the resulting image looks then "too good", because new "intermediate" intensity values are introduced. By using rounding to the nearest integer point all the intensity values on the map are real measurement results, which may help in understanding the whole observation better. In Figure A.4 there are two projections of a "chess board" image onto a map. The image C contained only black and white pixels —as can be seen in the map on the left which was produced without interpolation. The map on the right uses bi-linear interpolation to find the correct intensity, and the is result is apparently "better looking".

Appendix B

Measuring optical radiation

B.1 Irradiance, radiant intensity and radiance

In measuring optical radiation [*Jokela, 1992*] one often uses a quantity which describes the energy flow through an area in unit time. This quantity is called *irradiance* $[W/m^2]$:

$$E = \frac{d\Phi}{dA_d}, \tag{B.1}$$

where $d\Phi$ is the radiated power towards the area dA_d. When defined in this way E is a function of incident angle. Figure B.1 illustrates the situation.

Incoherent radiation very often contains components from different wavelengths and the spectral irradiance is

$$E_\lambda = \frac{dE}{d\lambda}, \tag{B.2}$$

of which we can integrate the total irradiance between $\lambda_1 \ldots \lambda_2$:

$$E = \int_{\lambda_1}^{\lambda_2} E_\lambda d\lambda \tag{B.3}$$

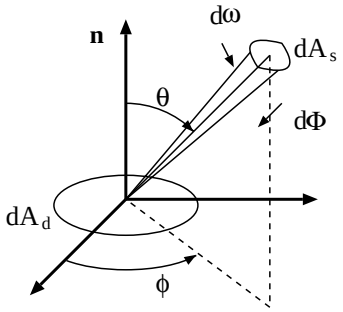

Figure B.1: Irradiance

The *radiant intensity* is the radiated power emitted per unit solid angle $[W/sr]$ and is defined as follows:

$$I = \frac{d\Phi}{d\omega}, \tag{B.4}$$

where $d\Phi$ is the radiated power into a solid angle $d\omega$. Correspondingly, the spectral radiant intensity $[W/(sr\, m)]$ is

$$I_\lambda = \frac{d\Phi_\lambda}{d\omega}. \tag{B.5}$$

The solid angle limited by the receiving surface dA and a point source at a distance r is

$$d\omega = \frac{dA\cos\theta}{r^2}, \tag{B.6}$$

and the power $d\Phi$ to the surface A_d by using (B.4) is $d\Phi = IdA\cos\theta/r^2$, from which follows that

$$E = \frac{d\Phi}{dA} = \frac{Icos\theta}{r^2}. \tag{B.7}$$

The equations presented here ignore any attenuation in the media.

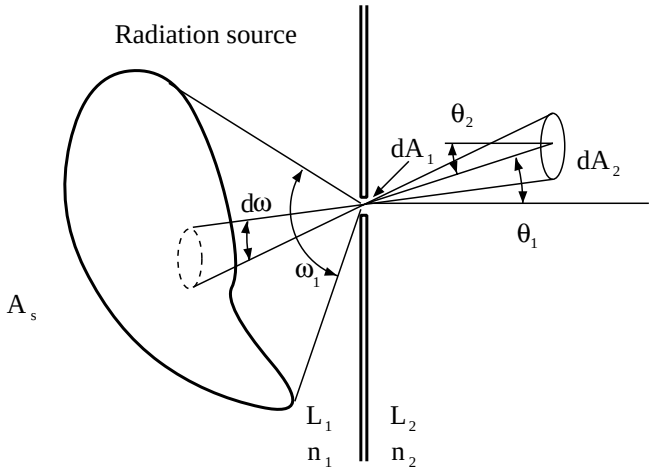

Figure B.2: Radiance

The *radiance* is the radiation from an extended source per unit solid angle and unit area $[W/(sr\, m^2)]$.

$$L_2 = \frac{d^2\Phi}{dA_1 \cos\theta_1 d\omega}, \tag{B.8}$$

where

$$d\omega = \frac{dA_2 \cos\theta_2}{r^2} \tag{B.9}$$

is the solid angle limited by the aperture dA_1. The term $dA_1 \cos\theta_1$ is the projection of the aperture in direction θ_1. If the system in Figure B.2 is lossless then

$$\frac{L_1}{n_1^2} = \frac{L_2}{n_2^2}, \tag{B.10}$$

where n_1 and n_2 are the refraction indices as indicated by Figure B.2.

Now, according to (B.8) the incoming power (aperture dA and solid angle $d\omega$) is $d^2\Phi = L\cos\theta dA d\omega$. By integrating the total power over the solid angle ω_1 limited by the source and dividing by the aperture dA we get from (B.1)

$$E = \frac{d\Phi}{dA} = \int_{\omega_s} L(\theta,\phi)\cos\theta d\omega, \tag{B.11}$$

where θ and ϕ are directional angles as seen in Figure B.1. Also, one can form the radiant intensity:

$$I(\theta,\phi) = \frac{d\Phi}{d\omega} = \int_{A_s} L(\theta,\phi)\cos\theta dA. \tag{B.12}$$

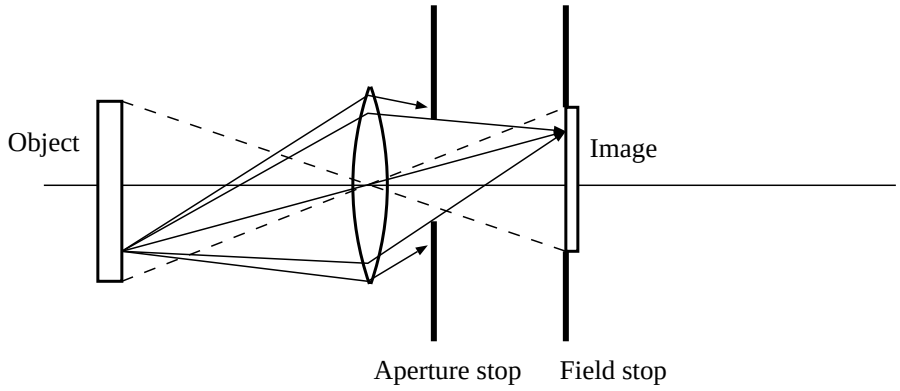

Figure B.3: Aperture and field stops

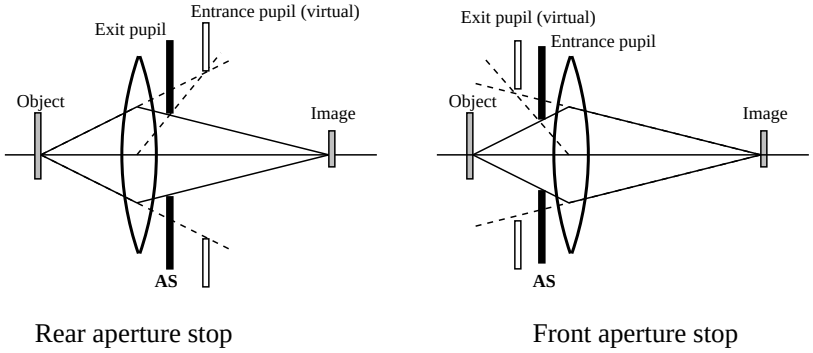

Figure B.4: Entrance and exit pupils

B.2 Optical terminology

In order to understand the system through which the incoming optical radiation is measured, some concepts of an optical system are very useful [*Hecht, 1987*]. Any element that limits the amount of light reaching the image is known as an *aperture stop* (AS). The field of view, on the other hand, is determined by the size of the *field stop* which determines the maximum image size, which usually is the size of the sensor. These stops are illustrated in Figure B.3. The aperture stop in the figure can also be called a *rear* aperture stop because of it location. If the stop is placed in front of the lens it is called a *front* aperture stop.

A *pupil* is the image of an aperture stop. The *entrance pupil* of a system is the image of the aperture stop as seen from an axial point on the object through those elements preceding the stop. The image can be virtual and magnified depending on the particular system, and it is always the "smallest" possible. The *exit pupil* is the image of the aperture stop as seen from an axial point on the image plane through the interposed lenses. Note that the entrance pupil alone limits the cone of light that enters the optical system. Figure B.4 illustrates the entrance and exit pupils in two cases with either a front aperture stop or a rear aperture stop.

A so called *f-number*, or $f/\#$ or $F\#$ is defined as

$$f/\# \equiv \frac{f}{D}, \tag{B.13}$$

where f is the focal length of the optical system and D is the diameter of the aperture[1]. If a system has an *f-number* of 2, it is usually designated $f/2$ or $F2$ respectively.

Numerical aperture (N.A.) is, by definition, the sine of the angle of the marginal ray makes with the optical axis:

$$\text{N.A.} = sin\theta = \frac{D}{2f} \tag{B.14}$$

Sometimes an optical system can be returned into an equivalent system consisting of two apertures that unambigously determine the input and output solid angles. If there is a third aperture somewhere in the system, because of which the effective aperture stop is narrower for an off-axis object point, a process called *vignetting* occurs. Due to vignetting the image points near its periphery "fade out" — the radiance decreases towards the edges of the image.

The surface, approximating a plane in the *paraxial region*[2], is called the *principal plane*. The *principal ray* is the ray that passes through the *principal points*, which are the points, where the principal planes intersect the optical axis. An optical system is called *telecentric* if the principal ray of all image-forming cones across the field of view cross the image plane parallel to the optical axis [*KeoConsultants, 1993*].

B.3 Sensor readings

A sensor converts the incoming radiance into an electrical quantity such as current or voltage. Generally the sensitivity of a sensor depends on the wavelength, the polarity, the power, the power distribution on the sensor area and the incident angle of the radiation. Thus, the spectral responsitivity is

$$R_\phi(x, y, \theta, \phi) = \frac{dS}{d\Phi}, \tag{B.15}$$

where $d\Phi$ is the incoming power to a surface dA, and

$$d^3\Phi = L_\lambda(x, y, \theta, \phi, \lambda) \cos\theta d\omega dA d\lambda. \tag{B.16}$$

where dS is the differential sensor output (voltage or current), L_λ is the spectral radiance at the wavelength $d\lambda$ and θ is the incident angle. If the output is current then the unit for spectral responsitivity is $[A/W]$. By combining and integrating (B.15) and (B.16) over the solid angle ω seen by the sensor, the sensor area A and the wavelength range $\Delta\lambda$, the output signal is

$$S = \int_{\Delta\lambda} \int_{A} \int_{\omega} R_\Phi(x, y, \theta, \phi, \lambda) L_\lambda(x, y, \theta, \phi, \lambda) \cos\theta d\omega dA d\lambda. \tag{B.17}$$

[1] This holds for circular lenses.

[2] The region where the light rays arrive at shallow angles with respect to the optical axis.

In practise one usually measures the "counts" per sensor per time, and this count depends not only on the incoming signal C_S but also on background radiation C_B, darkcount C_D and other disturbing sources C_M:

$$C_T = C_S + C_B + C_D + C_M, \tag{B.18}$$

Usually the sensor is an array of pixels, all of which can have different output values. Now, the measurent count of one pixel per unit time can be formulated as

$$\frac{C_S}{t} = \eta L_\lambda a \omega, \tag{B.19}$$

where η is the (effective) efficiency of the sensor, L_λ is the radiation from an extended or diffuse source larger than the field of view of the sensor pixel, a is the pixel area and ω is the solid angle seen by the pixel (see Figure B.8). Because the throughput of an optical system is invariant (see (B.10)) we can say that

$$A\Omega = a\omega, \tag{B.20}$$

where A is the effective area of the sensor aperture (which depends on all of the aperture stops in the optical system), a is the sensor pixel area and ω the solid angle seen by the pixel.

The signal-to-noise ratio or S/N is the ratio of the signal to the total noise, which is the uncertainity in the total photon count. Statistically the uncertainity of the total count is the fractional uncertainity $\sqrt{C}/C$, where C is the number of counts (Poisson statistics). $\sqrt{C}$ is the standard deviation in a group of samples collected over the same counting period.

$$\frac{S}{N} = \frac{C_S}{\sqrt{C_S + C_B + C_D + C_M}}, \tag{B.21}$$

which approaches the statistical uncertainity when $C_S \gg C_B + C_D + C_M$. By suitable hardware the effect of $C_D + C_M$ can be reduced, and sometimes the ratio C_S/C_B is used.

One can also use the f-number to formulate the measurement count by on pixel. The solid angle seen by the pixel is

$$\omega = \frac{A}{f^2} \tag{B.22}$$

$$= \frac{\pi D^2}{4 f^2}$$

$$= \frac{\pi}{4\, F^2}, \tag{B.23}$$

Now, the radiance by using the f-number is

$$\frac{C_S}{t} = \frac{\eta L_\lambda \pi a}{4\, F^2}. \tag{B.24}$$

As seen by (B.24) the sensor count is proportional to the inverse square of the f-number. Thus, the lower the f-number is the more light will enter the optical system.

Appendix C

Station software details

C.1 Dayschedule file

One example of the dayschedule file is given here. This file controls the imaging by providing necessary information to the ASC control routine. Each row is a *cycle*, and only one cycle can be run at a time. The first two parameters define the start and stop time of the imaging cycle, and the third parameter is the time interval between images. The last two parameters describe the exposure time and filter selection to be used. `GRE` is the only filter (557.7nm) in the prototype, and `DAR` means that the image should be a dark image ie. shutter will not be opened.

```
18:30:00 18:30:10 20 0500 DAR
18:30:20 19:59:20 20 0500 GRE
19:59:40 19:59:50 20 1000 DAR
20:00:20 20:04:40 20 1000 GRE
20:05:00 20:05:10 20 0800 DAR
20:05:20 20:10:00 20 0800 GRE
20:10:20 20:14:20 20 0500 GRE
20:14:40 20:14:50 20 0800 DAR
20:15:20 20:20:00 20 0800 GRE
20:20:20 20:20:35 20 0500 DAR
20:20:40 20:30:00 20 0500 GRE
20:30:20 20:30:35 20 0500 DAR
20:30:20 20:59:40 20 0500 GRE
21:00:00 21:00:10 20 0500 DAR
21:00:20 21:59:40 20 0800 GRE
22:00:00 22:59:40 20 0800 GRE
23:00:00 23:00:10 20 0800 DAR
23:00:20 23:59:40 20 0500 GRE
00:00:00 00:00:10 20 0500 DAR
00:00:20 05:30:00 20 0500 GRE
```

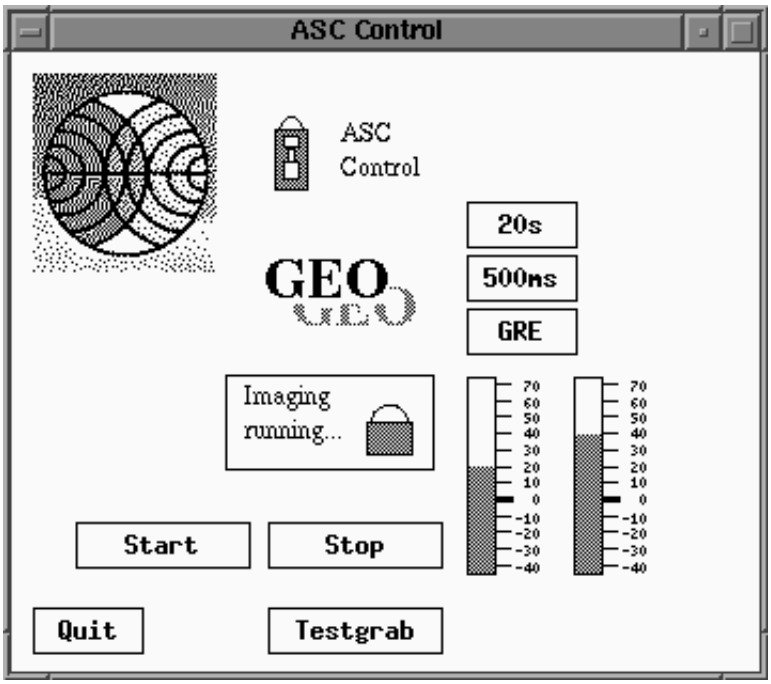

Figure C.1: ASC control user interface.

C.2 User interface

The user interface of the ASC control routine is shown in Fig. C.1. Starting and stopping of the image can be performed by mouse clicks, and the current state of the station is shown in the bitmap above `START` and `STOP` buttons. The two temperature bars to the right of the `STOP` button are only for evaluation purposes, because no temperature sensors were used in the prototype.

The three boxes above the temperature bars indicate the parameters of the cycle that is either the current cycle (if time is between the start and stop time of a cycle in the dayschedule) or the cycle that will be started next.

Some successful experiments were performed where the user interface process and the rest of the station software were distributed among two computers connected to the same network. Very few modifications to the station software were necessary, which supports the choice of Erlang as a programming language for the station network.

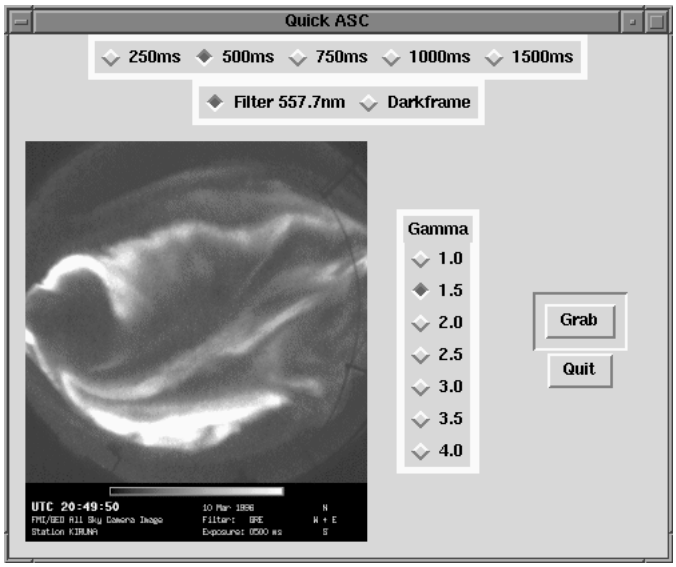

Figure C.2: Frame grabber routine.

C.3 Frame grabber routine front-end

The usage of the frame grabber control routine was made easier by experimenting with a TCL/TK (Tool Command Language/Tool Kit) script language. A graphical user interface was programmed which is shown in Fig. C.2. Testing imager settings and focusing the optics became quicker and more effortless.

Clicking the `GRAB` button executes a proper unix command, and the captured image is shown in half-size in the lower-left corner. By using the buttons the user can choose the exposure time and filter setting (again `GRE` or `DAR`). Various gamma corrections can be experimented by appropriate buttons, which is useful in case of dark aurorae.

The Erlang version that will be released this spring will support directly TCL/TK.